Geophys. J. Int. (2009) **178,** 1533–1554 doi: 10.1111/j.1365-246X.2009.04237.x

The 1956 earthquake and tsunami in Amorgos, Greece

Emile A. Okal,[1] Costas E. Synolakis,[2,3,4] Burak Uslu,[2,5] Nikos Kalligeris[3] and Evangelos Voukouvalas[3]

[1] *Department of Earth and Planetary Sciences, Northwestern University, Evanston,* IL 60208*, USA. E-mail: emile@earth.northwestern.edu*
[2] *Department of Civil Engineering, University of Southern California, Los Angeles,* CA 90089*, USA*
[3] *Department of Environmental Engineering, Technical University of Crete,* GR-73100 *Chania, Greece*
[4] *Institute of Applied and Computational Mathematics,* PO Box 1385, GR-71110 *Heraklion, Greece*
[5] *Pacific Environmental Laboratories, National Oceanographic and Atmospheric Administration,* 7600 *Sandpoint Way, Seattle,* WA 98105*, USA*

Accepted 2009 April 30. Received 2009 April 30; in original form 2008 January 31

SUMMARY

We conduct a comprehensive study of the Amorgos, Greece earthquake and tsunami of 1956 July 09, the largest such event in the Aegean Sea in the 20th century. Systematic relocation of the main shock and 34 associated events defines a rupture area measuring 75 × 40 km. The use of the Preliminary Determination of Focal Mechanism algorithm resolves the longstanding controversy about the focal geometry of the event, yielding a normal faulting mechanism along a plane dipping to the southeast, which expresses extensional tectonics in the back arc behind the Hellenic subduction zone. The seismic moment of 3.9×10^{27} dyn cm is the largest measured in the past 100 yr in the Mediterranean Basin.

A quantitative database of 68 values of tsunami run-up was built through the systematic interview, over the past 5 yr, of elderly eyewitness residents of 16 Aegean islands and the Turkish coast of Asia Minor. It confirms values of up to 20 m on the southern coast of Amorgos, 10 m on Astypalaia, and up to 14 m on the western coast of Folegandros, 80 km to the west of the epicentre. These values, largely in excess of the inferred seismic slip at the source, and their concentration along isolated segments of fault, are incompatible with the generation of the tsunami by the seismic dislocation, and require an ancillary source, in the form of a series of landslides triggered by the earthquake and/or its main aftershocks, a model confirmed by hydrodynamic simulations using both the dislocation source and models of landslide sources.

Keywords: Tsunamis; Submarine landslides; Europe.

1 INTRODUCTION

The earthquake of 1956 July 09 near Amorgos Island in the south-central Aegean Sea (Fig. 1) was the largest one to strike Greece in the 20th century, with a magnitude of 7.8, as computed by B. Gutenberg at Pasadena and reported by the International Seismological Summary (ISS). It resulted in 53 deaths and considerable damage, notably on the island of Santorini, and generated a local tsunami affecting the shores of the Cyclades and Dodecanese Islands, Crete and the Turkish coast of Asia Minor, with run-up values of 30, 20, and 10 m reported on the southern coast of Amorgos, on Astypalaia and Folegandros, respectively. Such values are the highest reported in the 20th century over the whole Mediterranean Basin (Solov'ev *et al.* 2000). This led Galanopoulos (1957) and later Ambraseys (1960) to propose a submarine landslide (or a series of landslides) as the source of the tsunami, based on the excessive amplitude and general heterogeneity of run-up in the epicentral area, properties later interpreted quantitatively by Okal & Synolakis (2004) as robust proxies for tsunamis of landslide origin in the near field.

The exceptional size of the Amorgos earthquake and the intriguing amplitude of its tsunami aroused the interest of the scientific community. Initial damage reports (Papastamatiou *et al.* 1956; Galanopoulos 1957) were interpreted by Papadopoulos & Pavlides (1992) and Stiros *et al.* (1994) in terms of the neotectonics of the island of Amorgos; Papazachos & Delibassis (1969), Shirokova (1972) and Ritsema (1974) proposed various conflicting focal mechanisms based on the compilation of *P*-wave first motions. The impact of the tsunami was described by Papazachos *et al.* (1985), its deposits on Astypalaia identified and dated by Dominey-Howes *et al.* (2000), and a hydrodynamic simulation proposed by Pedersen *et al.* (1995). Finally, Perissoratis & Papadopoulos (1999) mapped unstable marine sedimentary structures as potential sources of the tsunami.

In this context, we present here a comprehensive study of the 1956 Amorgos earthquake and tsunami, using modern techniques both in the seismological and hydrodynamic fields. Following the general approach of our previous study of the 1946 Aleutian earthquake (Okal *et al.* 2002, 2003; López & Okal 2006; Okal & Hébert 2007), we include the results of relocation of both the main shock and its

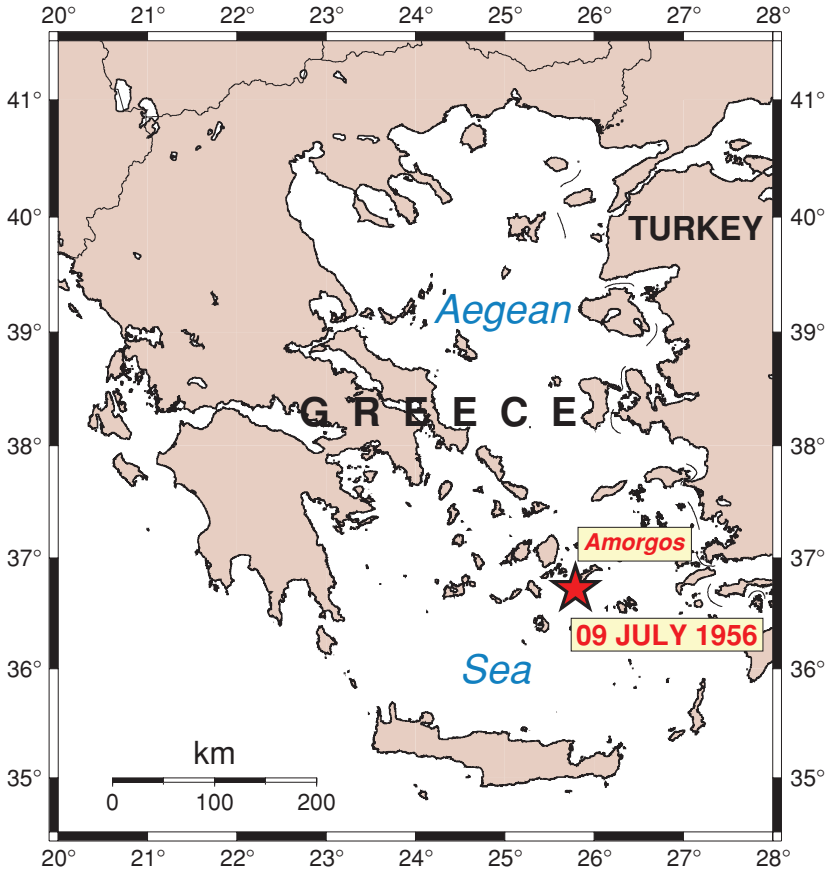

Figure 1. Situation map of the 1956 Amorgos earthquake.

aftershocks, a definitive focal solution obtained by moment tensor inversion of mantle surface waves, a database of 68 run-up values resulting from a series of systematic field surveys, and the results of numerical hydrodynamic simulations. We conclude that several underwater landslides must have been triggered by the earthquake, in order to explain the unusual run-up characteristics, notably along the southern coast of Amorgos and at Folegandros.

2 RELOCATION

We relocated the Amorgos main shock, one alleged foreshock and 34 associated events using the interactive, iterative method of Wysession *et al.* (1991), based on travel times listed by the ISS, or when not available, by the Bureau Central International de Séismologie (BCIS). For each event, a 95 per cent confidence ellipse was derived through a Monte Carlo algorithm injecting into the data set randomly generated Gaussian noise with a standard deviation $\sigma_G = 3$ s, appropriate for an earthquake in the 1950s. As discussed by Wysession *et al.* (1991), this procedure is a standard part of their algorithm, which estimates the confidence of the solution regardless of the non-linearity of the inversion. Relocation results are listed in Table 1 and summarized on Fig. 2. Note that hypocentral depth was irresolvable and therefore constrained at 30 km in all relocations. One event (labelled FC in Table 1) failed to converge.

Events 1–18, 23, 30 and 31 (shown in blue on Fig. 2) are interpreted as aftershocks, defining a probable rupture zone with average dimensions 75 km × 40 km, of which the main shock (36.72°N; 25.76°E; star on Fig. 2) occupies the northwestern corner, about 25 km from the relocation proposed by Engdahl & Villaseñor (2002). Of significant interest is the main aftershock (Number 1), occurring 12 min after the main shock, with a magnitude $M = 7.2$ (Uppsala), and which reportedly was responsible for most of the heavy damage and casualties on the island of Santorini (Thira). Our relocation in the neighbourhood of Anafi (36.39°N; 25.78°E; shown in red on Fig. 2) with a Monte Carlo ellipse approaching Santorini supports this interpretation, but does not necessarily require extending the fault zone to the west, as would be suggested by the location of the ISS epicentre, much closer to that island.

A southern cluster of events (19–22 and 24–29; shown in brown on Fig. 2), whose activity starts on 1956 July 28, constitutes a separate group, possibly expressing seismicity triggered on a different fault system by a mechanism of stress transfer (Stein *et al.* 1997). Event 32, occurring southeast of Karpathos (shown in grey on Fig. 2) may not be part of the Amorgos sequence. Event X1 (occurring 14 hr before the main shock) relocates near Lesvos, and Event X2 in the South Peloponessis; both locations are 260 km from the main shock, and outside the range of Fig. 2. These earthquakes are most probably unrelated to the Amorgos event.

3 FOCAL MECHANISM

Various authors have proposed focal mechanisms for the Amorgos earthquake, which generally fall into two classes (see Fig. 3). Papazachos & Delibassis (1969) and Ritsema (1974) have suggested mostly strike-slip solutions, while Shirokova (1972) proposed a normal faulting geometry more readily interpretable in the local tectonic context (Papadopoulos & Pavlides 1992). The origin of this discrepancy remains obscure, since only Shirokova (1972)

Table 1. Relocation of main shock and associated seismicity.

Number	Date				Relocation results					Published magnitude[a]
	D	M	(J)	Y	Time (GMT)	Latitude (°N)	Longitude (°E)	Number of stations	σ (s)	
MAIN	09	JUL	(191)	1956	03:11:45	36.72	25.76	253	3.27	7.8
1	09	JUL	(191)	1956	03:24:07	36.39	25.78	50	2.36	7.2
2	09	JUL	(191)	1956	04:15:14	36.49	25.95	9	4.69	5.0
3	09	JUL	(191)	1956	04:33:25	36.66	26.01	24	2.10	$5^1/_4$
4	09	JUL	(191)	1956	05:14:13	36.31	25.79	14	1.98	
5	09	JUL	(191)	1956	06:19:12	36.62	25.75	50	2.21	
6	09	JUL	(191)	1956	06:22:51	36.69	25.78	48	1.36	
7	09	JUL	(191)	1956	07:36:32	36.53	25.69	23	2.09	$5^1/_2$
8	09	JUL	(191)	1956	09:45:10	36.50	25.86	31	2.82	5.1
9	09	JUL	(191)	1956	11:30:53	36.41	26.30	27	2.06	
10	09	JUL	(191)	1956	20:10:28	36.66	26.11	32	2.06	5.0
11	09	JUL	(191)	1956	20:13:57	36.70	25.97	58	2.62	
12	09	JUL	(191)	1956	20:48:04	36.45	26.99	25	3.57	
13	09	JUL	(191)	1956	21:28:45	36.54	25.97	41	1.91	
14	10	JUL	(192)	1956	00:28:37	36.61	26.01	11	2.41	
15	10	JUL	(192)	1956	01:59:41	36.67	26.40	34	2.70	
16	10	JUL	(192)	1956	03:01:29	36.70	26.22	68	1.62	
17	12	JUL	(194)	1956	06:17:49	36.64	25.93	8	1.49	
18	22	JUL	(204)	1956	03:29:02	36.88	26.34	56	2.15	
19	28	JUL	(210)	1956	15:19:00	35.93	26.09	9	1.54	
20	30	JUL	(212)	1956	05:41:05	35.83	26.01	51	2.72	5.5
21	30	JUL	(212)	1956	05:47:13	35.88	25.88	17	2.13	
22	30	JUL	(212)	1956	09:15:02	35.87	25.95	94	2.87	6.0
23	30	JUL	(212)	1956	09:21:26	36.20	25.60	18	2.69	$5^1/_4$
24	30	JUL	(212)	1956	10:40:01	35.83	25.93	54	2.48	
25	09	AUG	(222)	1956	03:37:09	35.94	26.25	15	1.97	
26	06	SEP	(250)	1956	11:46:40	35.67	25.86	63	2.83	
27	06	SEP	(250)	1956	12:58:43	35.92	25.89	25	3.05	
28	16	SEP	(260)	1956	18:07:41	35.91	26.00	49	2.75	
29	29	OCT	(303)	1956	07:35:02	35.78	26.41	21	3.56	$5^1/_4$
30	02	DEC	(337)	1956	19:41:17	36.45	25.90	14	3.57	$5^1/_4$
31	09	FEB	(030)	1957	01:39:36	36.70	26.63	13	2.32	$5^1/_4$
32	06	MAR	(065)	1957	17:34:14	35.24	27.39	16	2.75	
X1	08	JUL	(190)	1956	13:05:24	39.09	26.17	21	7.00	5.0
X2	10	JUL	(192)	1956	23:37:24	36.30	22.89	26	2.60	
Failed to converge (FC)										
FC	29	OCT	(303)	1956	06:59					

[a]Magnitudes as compiled in the USGS database; all values are reported by Athens Observatory, with the exception of the main shock (reported by Pasadena) and Event 1 (reported by Uppsala).

published individual first motion polarities, while the other two studies (whose authors did collaborate) reported only the results of computer optimizations of undisclosed data sets.

In view of this controversy, we investigated the focal mechanism of the Amorgos earthquake using the Preliminary Determination of Focal Mechanism (PDFM) algorithm introduced by Reymond & Okal (2000), which inverts mantle Rayleigh and Love waves, but uses only spectral amplitudes, disregarding the phase information in the seismograms. For this reason, and as shown by Okal & Reymond (2003), the method is particularly useful to resolve the moment tensors of historical earthquakes, since it is insensitive to errors in the relative timing between stations; it can be applied successfully to data sets consisting of as few as three stations, as long as they provide adequate azimuthal coverage. However, as originally explained by Romanowicz & Suárez (1983), the method involves a double 180° indeterminacy in strike and slip angles, which can be lifted only by independent observations, such as polarities of body waves at critical stations.

In this instance, we used first passages of Rayleigh and Love waves, R_1 and G_1, recorded on the Pasadena (PAS) Benioff 1–90 seismometer (which can be regarded as a prototype of more recent broad-band systems), on its close 1–60 relative at Weston (WES), and on the Wenner and Milne-Shaw instruments at San Juan (SJG) and Honolulu (HON), respectively, these four stations providing an optimal aperture of 88° in azimuth. A representative record is shown on Fig. 4. The data set of spectral amplitudes at periods of 100–200 s converges on a moment of $M_0 = 3.9 \times 10^{27}$ dyn cm; a centroid depth of 45 km minimizes residuals. This relatively deep value would in general agree with the observation of maximum Modified Mercalli Intensities not exceeding IX on the island of Amorgos despite the large magnitude of the event (Papastamatiou *et al.* 1956; Ambraseys & Jackson 1990; Papadopoulos & Pavlides 1992); this centroid estimate also agrees well with Engdahl & Villaseñor's (2002) hypocentral depth of 35 km.

The indeterminacy between the four possible mechanisms shown on Fig. 5 is lifted by the following polarity constraints: first motion *P* up and *S* to north at WES; first motion *P* down and $SH > SV$ at Almaty, Kazakstan (AAA; see Fig. 6); diffracted *P* down at PAS; and *S* recorded stronger on NS than EW at SJG. The final solution, shown on Fig. 3, corresponds to case I of Fig. 5, and features

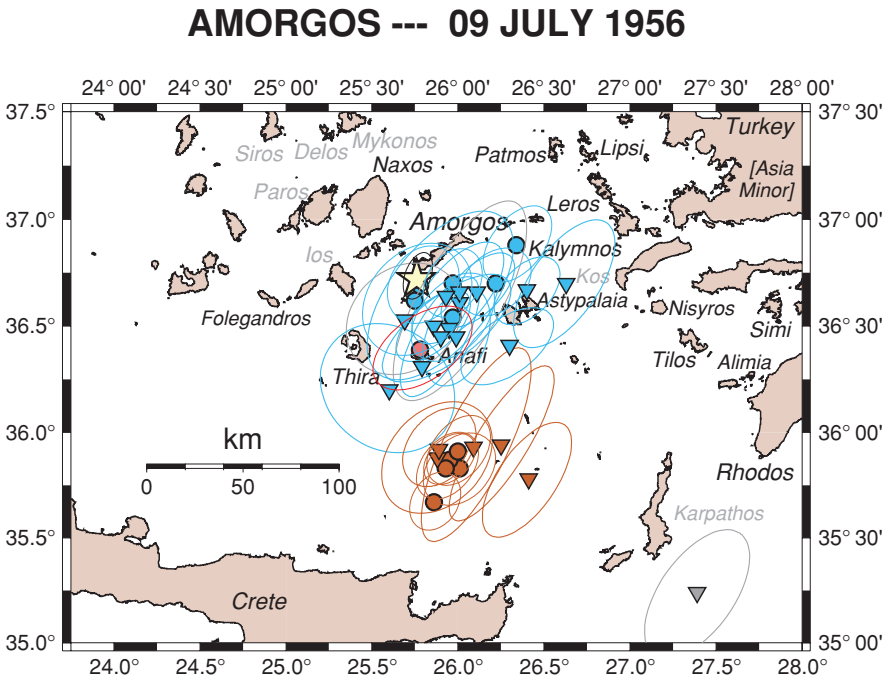

Figure 2. Close-up of Fig. 1 showing the results of our relocations and mapping the sites of the field survey. Islands visited during the tsunami field survey are named in black (e.g. Folegandros); other islands are referenced in grey (e.g. Karpathos). For each relocated event (see Table 1), the Monte Carlo ellipse ($\sigma_G = 3$ s) is shown. The main shock is plotted as the large star, events listed in the ISS as circles, and events listed only by the BCIS as inverted triangles. Aftershocks defining the extent of rupture are shown in blue, events from the southern cluster in brown. The main aftershock at 03:24 is shown in red.

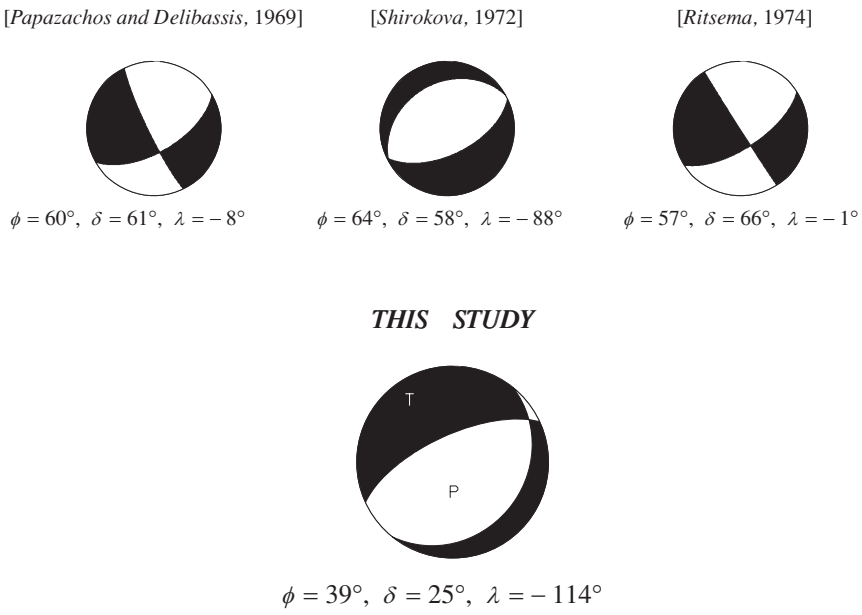

Figure 3. Top panels: focal mechanisms previously published for the 1956 Amorgos earthquake. Bottom panel: preferred solution inverted using the PDFM method.

a normal faulting mechanism in general agreement with that of Shirokova (1972), the solid rotation between the two being only 37° in the formalism of Kagan (1991). It is generally incompatible with the strike-slip class of solutions, being, for example, rotated as much as 91° from Ritsema's (1974), and 96° from Papazachos & Delibassis' (1969). Note that the asymmetry of the final focal mechanism, with the two fault planes dipping 25° and 67°, respectively (as opposed to the more symmetric value of 45° characteristic of a standard, textbook normal faulting earthquake), is a robust feature necessary to match the observed low amplitude of Love waves, relative to their stronger Rayleigh counterparts.

This focal mechanism can be interpreted as nearly pure normal faulting with either a small component of right-lateral motion on a fault dipping gently to the SSE ($\phi = 39°$; $\delta = 25°$; $\lambda = 246°$), or of left-lateral slip on the conjugate fault dipping more steeply to the NNW ($\phi = 245°$; $\delta = 67°$; $\lambda = 281°$). Unfortunately, we could

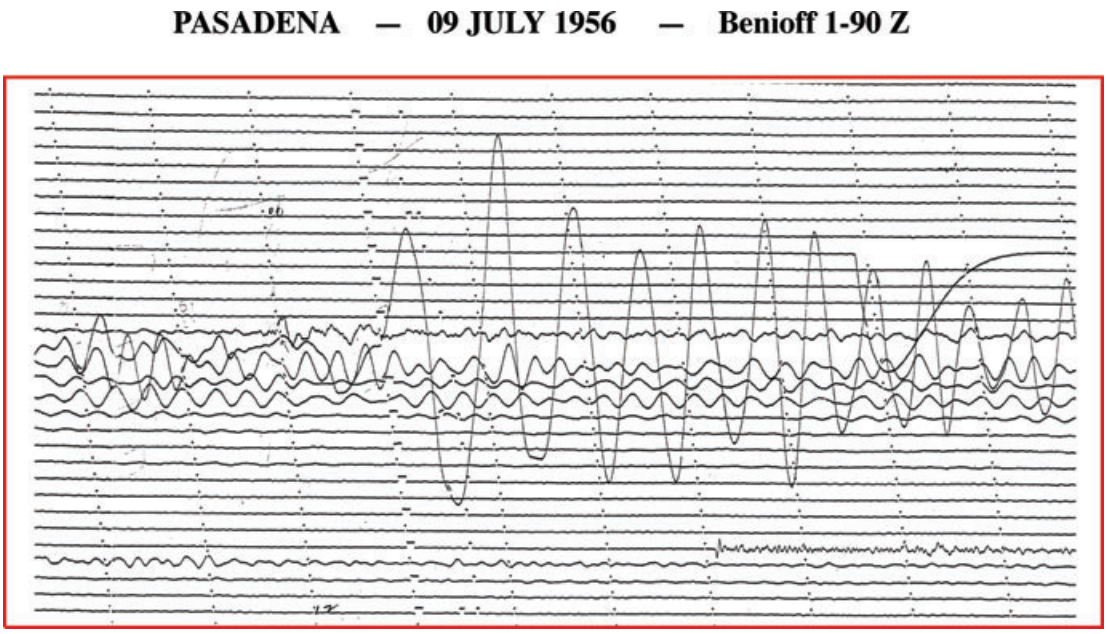

Figure 4. Example or record used in the PDFM inversion. This is the Rayleigh wave R_1 recorded on the vertical Benioff 1–90 instrument at Pasadena.

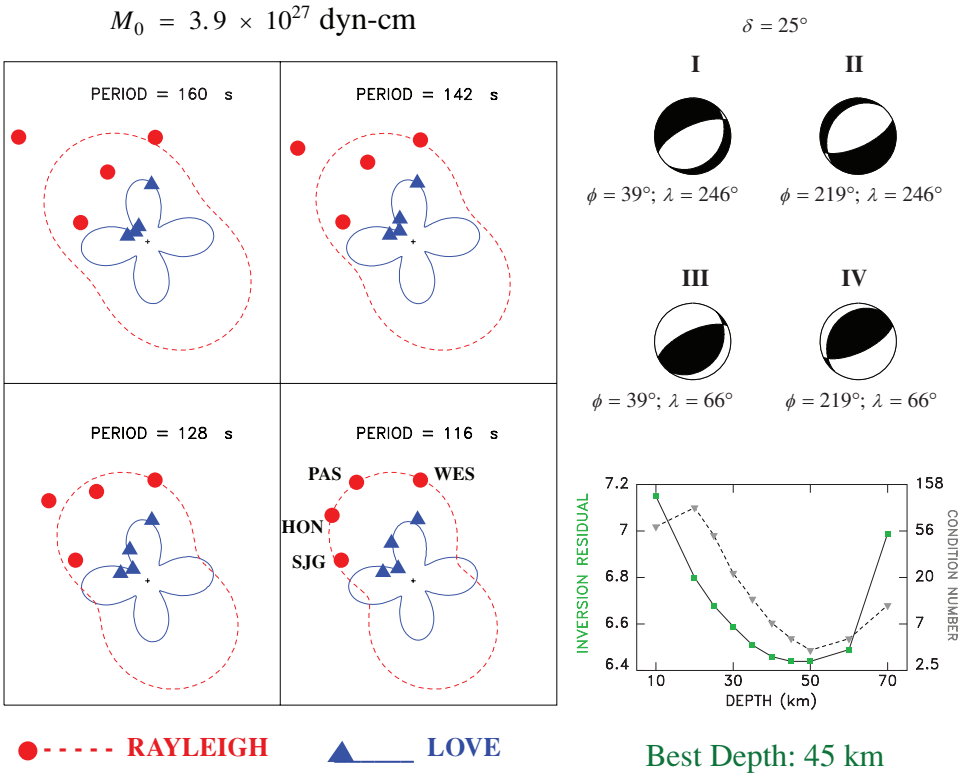

Figure 5. Results of the PDFM inversion. Left-hand panels: azimuthal fits of inverted spectra at the four stations used, for a representative set of periods. The solid (Love) and dashed (Rayleigh) lines are the theoretical spectral amplitudes, the dots (Rayleigh) and triangles (Love), the observed values. The scales are common in each box, but vary with period. Top right-hand panels: sketch of the four possible focal mechanisms corresponding to the inverted solution. Bottom right-hand panel: variation with source depth of the inversion residual (solid line and square symbols; left scale in arbitrary units). Its minimum around 45 km is interpreted as the centroid of rupture. It is also close to the minimum in the condition number of the data set (dashed lines; inverted triangles, right (logarithmic) scale).

not find reports of surface faulting during the Amorgos earthquake (which would help resolve the fault plane); significantly, the event is absent from Ambraseys & Jackson's (1998) authoritative compilation of such observations for the Eastern Mediterranean Basin, a probable effect of its combined source depth and epicentral location at sea.

On the other hand, the repartition of aftershocks (Fig. 2) clearly favours the former model of a fault dipping gently (25°) to the

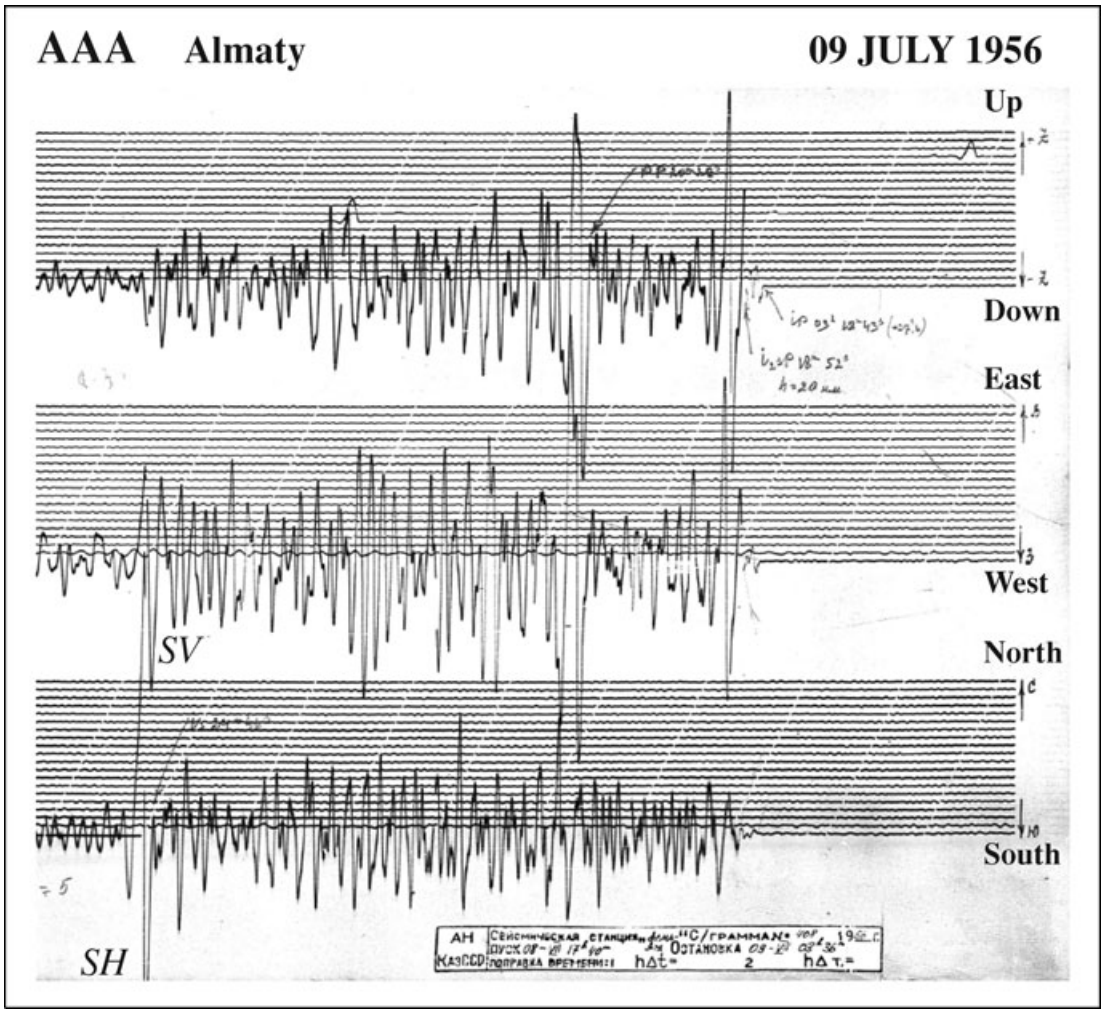

Figure 6. Close-up of 3-D record at Almaty, Kazakstan (AAA). Time increases to the left. For this naturally polarized station (backazimuth $\beta = 278^\circ$), we clearly observe a dilatational *P* wave and $SH/SV > 1$.

SSE, which we therefore adopt as the focal mechanism of the 1956 Amorgos earthquake. In order to investigate the static displacement produced in the epicentral area by the preferred source, we interpret the seismic moment M_0 using seismic scaling laws (Geller 1976), to derive a fault length $L = 81$ km, a fault width $W = 41$ km, and a seismic slip $\Delta u = 2.46$ m. Note that the dimensions of the fault are in agreement with those of the aftershock zone. These parameters are then used to build a field of static displacements of the Earth's surface, using Mansinha & Smylie's (1971) algorithm, which is equivalent to Okada's (1985) for a Poisson solid half-space. These values are mapped on Fig. 7, and will be considered as the field of initial displacement of the sea surface in our hydrodynamic simulations (see Section 5).

The results shown on Fig. 7 are in agreement with the quaternary tilting of Amorgos island, but predict a net coseismic subsidence of the island (on the order of 20 cm), rather than the general interpretation of Quaternary uplift of its southern shore prevailing in the geomorphological literature (Papadopoulos & Pavlides 1992; Stiros *et al.* 1994). In particular, Stiros *et al.* (1994) have analysed fossil vermet deposits on the southeastern coast of Amorgos suggestive of rapid coastal uplift, and used a comparison between airborne photographs taken in 1945 and 1960 to suggest that this uplift occurred during the 1956 earthquake. In turn, these authors have proposed an elastic deformation model consistent with normal faulting, and predicting a coseismic uplift of 30 cm along the southern coast of Amorgos (their Fig. 5), rather than the subsidence computed on Fig. 7.

However, this result is entirely controlled by their use of a dip angle of 45°, and of a probable shallow hypocentre for their dislocation (they do not report that particular parameter of their model, but we required a value of 10 km to be able to reproduce their profile). As discussed above, the surface wave inversion requires a mechanism departing from a dip of 45°, and a generally deeper source, the latter also suggested by Engdahl & Villaseñor's (2002) relocation. The use of the conjugate plane of the preferred solution ($\phi = 39^\circ$; $\delta = 25^\circ$; $\lambda = 246^\circ$) would also lead to subsidence on the southern coast of Amorgos (and at any rate, is incompatible with the aftershock distribution). Finally, in order to position the southern shore of Amorgos into the area of uplift of Fig. 7, we could globally move the whole source to the NNW, but at least 35 km, which is beyond the uncertainty of our relocation.

In order to reconcile our results with the field evidence and the photographic interpretations of Stiros *et al.* (1994), we speculate that the uplift which they have documented may not have taken place coseismically, but rather aseismically, possibly as a result of the activation of secondary, shallower and steeper faults, in the weeks

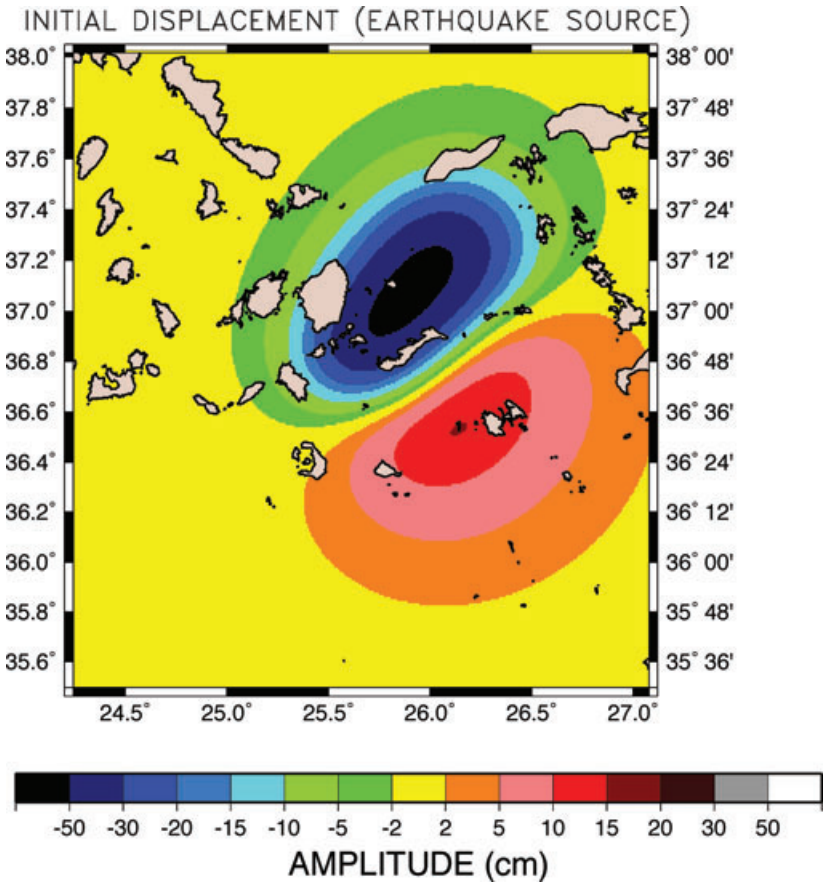

Figure 7. Field of static displacement created by the seismic source inverted in Section 3, obtained using the algorithm of Mansinha & Smylie (1971). These values are used as the initial condition of the hydrodynamic solution under the earthquake scenario.

or months following the 1956 earthquake (but before the second airborne photograph was taken in 1960).

In conclusion of this section, and on a more regional scale, our mechanism confirms the interpretation of the Amorgos earthquake as expressing backarc extensional tectonics (the tension axis striking N327°E) in the general framework of subduction at the Hellenic trench (McKenzie 1978; Le Pichon & Angelier 1979; Taymaz *et al.* 1991).

4 TSUNAMI FIELD SURVEY

While many descriptions of the effects of the Amorgos tsunami were published in the early works of Galanopoulos (1957) and Ambraseys (1960), they consisted mostly of second-hand reports and lacked exact coordinates for the relevant sites. In this context, we conducted a field survey of the 1956 Amorgos tsunami to obtain a quantitative database of run-up and inundation values, based on recorded testimony from elderly witnesses, a technique which we pioneered in the case of the 1946 Aleutian tsunami in the Pacific Ocean (Okal *et al.* 2002, 2003; Okal & Hébert 2007). After interviewing individual witnesses, the exact extent of penetration of the wave was surveyed (usually in the presence of the witness) using classical topographic methods, to obtain 'inundation', defined as the horizontal extent of maximum penetration of the wave, and 'run-up', defined as the altitude above unperturbed sea level, at the point of maximum penetration (Synolakis & Okal 2005). The resulting data set is listed in Table 2 and presented on Figs 8(a)–(m). It represents a coherent quantitative database with each point surveyed using GPS techniques. No tidal corrections were effected since tidal amplitudes are negligible in the essentially landlocked Mediterranean Basin, and especially so in the Aegean Sea, where the tidal excursion does not exceed 10 cm.

Notwithstanding the systematic difficulties associated with interpreting memories of the time of occurrence of events, we asked witnesses to give us their best estimates of the arrival times of the waves. We detail here instances of what we believe are intriguing reports of the timing of the tsunami waves. In this respect, we note that the earthquake took place at 03:11 GMT, or 05:11 local time (like most of Europe, Greece did not adopt Daylight Saving Time in the Summer until the mid 1970s). More importantly, as solar time in the islands was about 04:55, that is, past sunrise on one of the longest days of the year, the earthquake was felt and the tsunami arrived at all sites in daylight.

Amorgos; Sites 1–7; Fig. 8(a).

Seven points were surveyed during our visit to Amorgos in 2003 August. The most interesting data point is at Mouros (Site 6), where we measured a run-up of 20 m, based on the testimony of two retired shepherds, aged 33 and 18, respectively, in 1956, and whom we interviewed independently of each other. Both eyewitnesses described the phenomenon as featuring a leading depression (initial withdrawal of the sea), which took place 'within minutes of the earthquake'.

There are no villages on the eastern coast of Amorgos, which falls abruptly into the sea along a mostly linear shoreline. The only other location providing some insight into the effect of the tsunami

Table 2. Run-up data set obtained during field survey.

Site number	Latitude (°N)	Longitude (°E)	Run-up (m)	Island	Site and notes
1	36.901615	25.977066	2.5	Amorgos	Ormos Aigialis
2	36.904316	25.978149	1.0	Amorgos	Ormos Aigialis
3	36.878235	25.931616	2.5	Amorgos	Agios Pavlos
4	36.825565	25.905884	9.7	Amorgos	Agia Anna
5	36.830750	25.867216	1.5	Amorgos	Katapalo
6	36.785900	25.830183	20.0	Amorgos	Mouros
7	36.805534	25.783199	1.5	Amorgos	Katokampos
8	36.570435	26.356133	7.0	Astypalaia	Stavros
9	36.542549	26.342884	2.5	Astypalaia	Livadia, vacant lot
10	36.576935	26.389584	1.2	Astypalaia	Maltezana, eastern end of beach
11	36.576683	26.385000	2.2	Astypalaia	Maltezana, Swamp east of hotel
12	36.575401	25.383699	2.0	Astypalaia	Maltezana, Road to beach
13	36.574234	26.383167	3.0	Astypalaia	Maltezana, western end of beach
14	36.587234	26.404083	7.5	Astypalaia	Vai, Cave on cliff
15	36.605499	26.398899	4.0	Astypalaia	Bay 1, Below house at end of road
16	36.620483	26.394184	3.0	Astypalaia	Vathi, Road above taverna
17	36.548901	26.353201	2.6	Astypalaia	Skala, Blockhouse in front of school
18	36.548584	26.352800	4.0	Astypalaia	Skala, interpreted from postcard
19	36.570435	26.357483	10.0	Astypalaia	Stavros, DH Point 2
20	36.541100	26.339634	2.0	Astypalaia	Livadia, DH point 1
21	36.356266	25.475283	3.0	Santorini	Perissa, shops on waterfront
22	36.336266	25.436516	2.0	Santorini	Vlichada, waterfront
23	36.344601	25.771067	3.0	Anafi	Agios Nikolaos, steps near parked car
24	36.615501	24.948166	1.3	Folegandros	Karavostasis, Port
25	36.630932	24.894117	12.6	Folegandros	Aggali, Ex-river bed
26	36.630199	24.884600	3.1	Folegandros	Agios Nikolaos, Beach
27	36.650234	24.845900	14.6	Folegandros	Ambeli, Splash on cliff behind beach
28	36.664616	24.859983	1.1	Folegandros	Agios Georgios, Beach
29	36.937433	25.473683	1.2	Naxos	Kalantos, flat terrain
30	36.958933	25.539467	1.6	Naxos	Panormos
31	36.986750	25.559733	1.9	Naxos	Kleidos 1
32	36.990117	25.559400	2.3	Naxos	Kleidos 2
33	37.007700	25.567450	2.1	Naxos	Zo
34	37.017367	25.572117	3.1	Naxos	Kanakis
35	37.078617	25.587217	3.1	Naxos	Moutsouna
36	37.181983	25.551983	2.0	Naxos	Apollonas
37	37.103800	25.374900	2.0	Naxos	Chora Naxou
38	37.070067	25.353917	2.1	Naxos	Agia Anna
39	36.987017	25.391767	1.8	Naxos	Glyfada Beach
40	35.488950	24.060833	1.5	Crete	Chania Souda In. 250
41	35.341650	25.135867	2.0	Crete	Iraklion Inun 30
42	35.190700	25.718883	1.5	Crete	Agios Nikolaos Inun. 5
43	35.264033	25.719317	1.5	Crete	Agios Nikolaos Elunta In. 150
44	37.354924	26.540595	3.0	Patmos	
45	37.350042	26.565976	3.0	Patmos	Agriolivado
46	37.302541	26.561283	1.7	Patmos	
47	37.295479	26.767131	3.0	Lipsi	Wharf destroyed
48	37.152485	26.828033	4.0	Leros	Gourna
49	37.131248	26.854233	2.0	Leros	Laki, Cycle shop
50	37.132351	26.852716	2.7	Leros	Laki, Statue
51	36.949663	26.985553	2.0	Kalymnos	Boat sunk
52	36.61390	27.13845	2.9	Nisyros	Mandraki, post office
53	36.61172	27.13223	3.7	Nisyros	Mandraki, KlearchouKourouni str.
54	36.45925	27.33533	2.5	Tilos	Agios Antonios, Tavern
55	36.41678	27.38562	0.8	Tilos	Livadia, older dock
56	36.43347	27.34763	3.1	Tilos	Eristos, sand dune
57	36.43433	27.34793	2.2	Tilos	Eristos, Hotel Ereisos
58	36.54832	27.84643	2.4	Symi	Panormitis, Monastery
59	36.61562	27.85550	1.1	Symi	Pedi, entrance to tavern
60	36.61418	27.85546	1.3	Symi	Pedi, Agios Georgios church
61	36.26860	27.71128	2.1	Alimia	Agios Georgios Church
62	35.89208	27.77338	2.1	Rhodos	Prasonissi, Mini Market

Table 2. (*Continued*.)

Site number	Latitude (°N)	Longitude (°E)	Run-up (m)	Island	Site and notes
63	37.396332	27.212116	1.1	Turkey	Didyma Ibrahim
64	37.392250	27.218033	1.5	Turkey	Didyma-Kizilyer, Beach
65	37.105518	27.292866	1.8	Turkey	Yalıkavak, River Bed
66	37.106098	27.292984	1.1	Turkey	Yalıkavak, Town
67	37.113918	27.292833	2.1	Turkey	Yalıkavak, Suburb
68	37.042885	27.431667	1.0	Turkey	Bodrum Town Hall

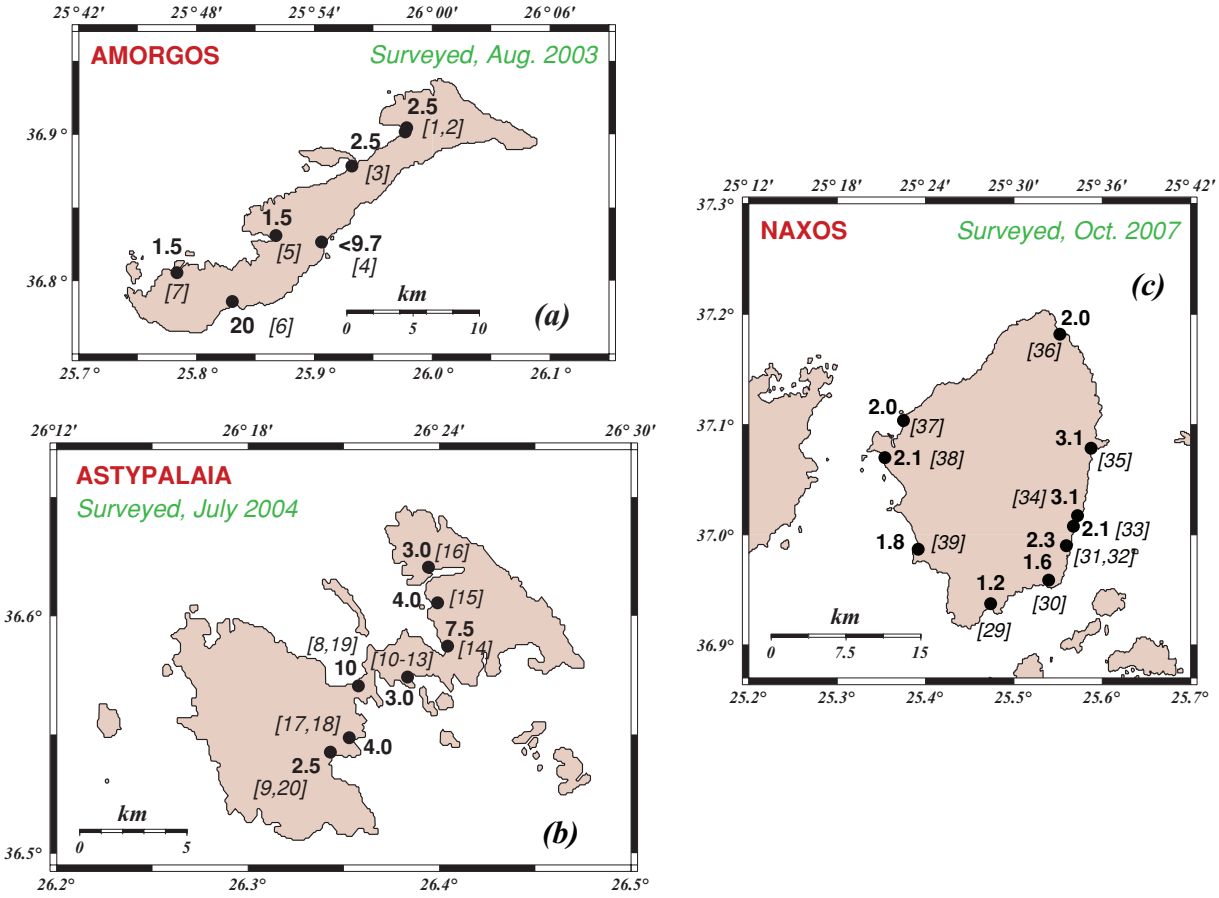

Figure 8. (a) Map of the island of Amorgos showing sites of the tsunami survey. At each location, the bold number (e.g. **2.7**) is the measured run-up in meters. The bracketed number in italics (e.g. *[3]*) is the site number as reported in Table 2. In case of two sites closer than the size of the dots on the scale of the map, only the largest run-up is printed. (b) Same as (a) for Astypalaia. (c) Same as (a) for Naxos. Survey maps for Folegandros (d), Santorini (e) and Anafi (f). Survey maps for Nisyros and Tilos (g), Crete (h) and Symi, Amilia and Rhodos (i). Survey maps for Patmos and Lipsi (j), Leros (k) and Kalymnos (l). (m) Survey map for the southwestern Coast of Turkey (Asia Minor). The open triangle shows the position of the virtual gauge used for the simulation shown on Fig. 12, at the entrance to the bay of Yalıkavak.

on that coast is Site 4, the small chapel of Agia Anna, which we surveyed at an altitude of 9.7 m. As several testimonies, including that of the former mayor of the island, established that the chapel was unaffected by the tsunami, this data point provides an upper bound for the run-up. At the other sites on Amorgos, all located on the western shore of the island, run-up did not exceed 2 m.

The data point at Site 6 revises downward the published value of 30 m for Amorgos, but confirms an exceptionally large run-up value (more than eight times the estimated slip Δu on the fault) along an essentially straight shoreline, unaffected by large embayments and promontories. Furthermore, the upper bound obtained at Site 4, only 8 km away from Mouros, requires a very rapid decay of the run-up along the shoreline. In the near field, both observations are incompatible with the generation of the tsunami by a standard double-couple source (Okal & Synolakis 2004), and thus they strongly support a triggered underwater landslide as the source of the large tsunami waves observed along the southern coast of Amorgos.

Astypalaia; Sites 8–20; Fig. 8(b).

This butterfly-shaped island is located 40 km SE of Amorgos, across the Amorgos Basin, at the southern end of the probable extent of the fault zone of the 1956 main shock. We obtained a total of 13 data points at seven main sites on the island. The other sections of the island are undeveloped and difficult to access. In very general

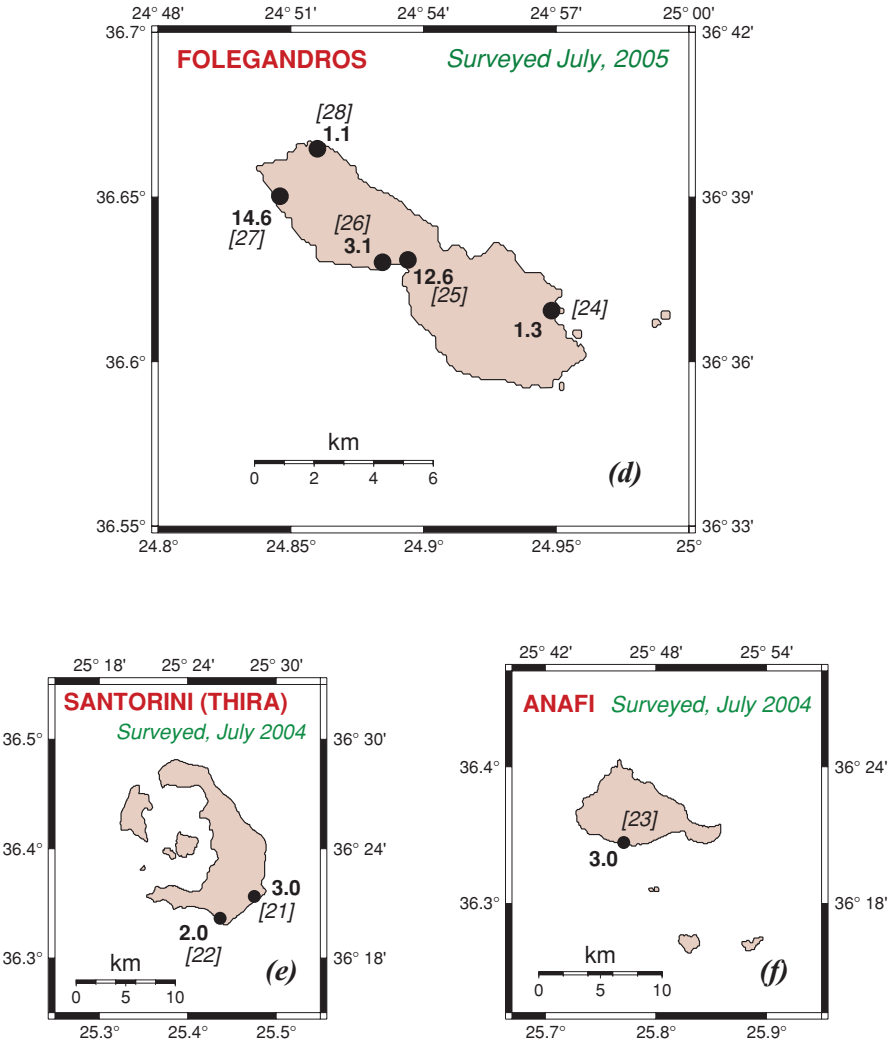

Figure 8. (*Continued*.)

terms, run-up was contained to 4 m or less on the southern coast of the island where most of the villages are located (Livadia, Skala, Maltezana). This was sufficient to result in inundation distances reaching 285 m in the alluvial plain at Livadia (Site 9) and 70 m at Maltezana. On the northern side of the island, we were able to recognize the deposits described by Dominey-Howes *et al.* (2000), 10 m above sea level on an outcrop of the Stavros isthmus (Site 19). Five km to the east, in the Bay of Vai, the tsunami penetrated inland at least 700 m, corresponding to a run-up of 7.5 m. Further north on the eastern peninsula (the right wing of the butterfly), the run-up drops back to 4 and 3 m at the unnamed Bay '1' (Site 15) and at Vathy, respectively.

Naxos; Sites 29–39, Fig. 8(c).

The highest run-up values were found on the eastern coast of the island with a maximum at Moutsouna (3.1 m; Site 35), decaying slowly southwards to 1.6 m at Panormos (Site 30); all eyewitnesses reporting an initial down-draw. By contrast, on the western shore, run-up values were fairly constant and generally smaller, ranging from 1.8 to 2.1 m; two eyewitnesses in different locations reported a leading elevation wave. In Chora Naxou (Site 37), eyewitnesses described waves coming from two directions, first from the south, then from the north. In Apollonas, at the northern tip of Naxos, run-up was measured at 2 m, but the polarity of the initial wave was unclear. In Kalantos at the southern tip, the flat topography resulted in an extreme inundation of more than 100 m inland for a moderate run-up of only 1.2 m.

Santorini; Sites 21–22; Fig. 8(e).

We surveyed two points on the southern coast of the island, at Perissa and Vlichada, respectively. In general, the tsunami did relatively little damage, especially as compared with the earthquakes (especially the 03:23 aftershock), which destroyed many buildings including the church at Perissa. Run-up on the beach was in the 2–3 m range.

Anafi; Site 23; Fig. 8(f).

We obtained testimonies from a total of nine eyewitnesses on this island, and surveyed one data point in the port village of Agios Nikolaos on the southern coast of the island, where run-up was 3 m. One of the witnesses estimated a flow depth of 3–4 m over a house at Vrissi, on the north shore, but this site could not be visited. The witnesses described the 'second earthquake', that is, the main aftershock at 03:23 GMT as felt strongest, which agrees with our relocation of that smaller event in the immediate vicinity of the island of Anafi.

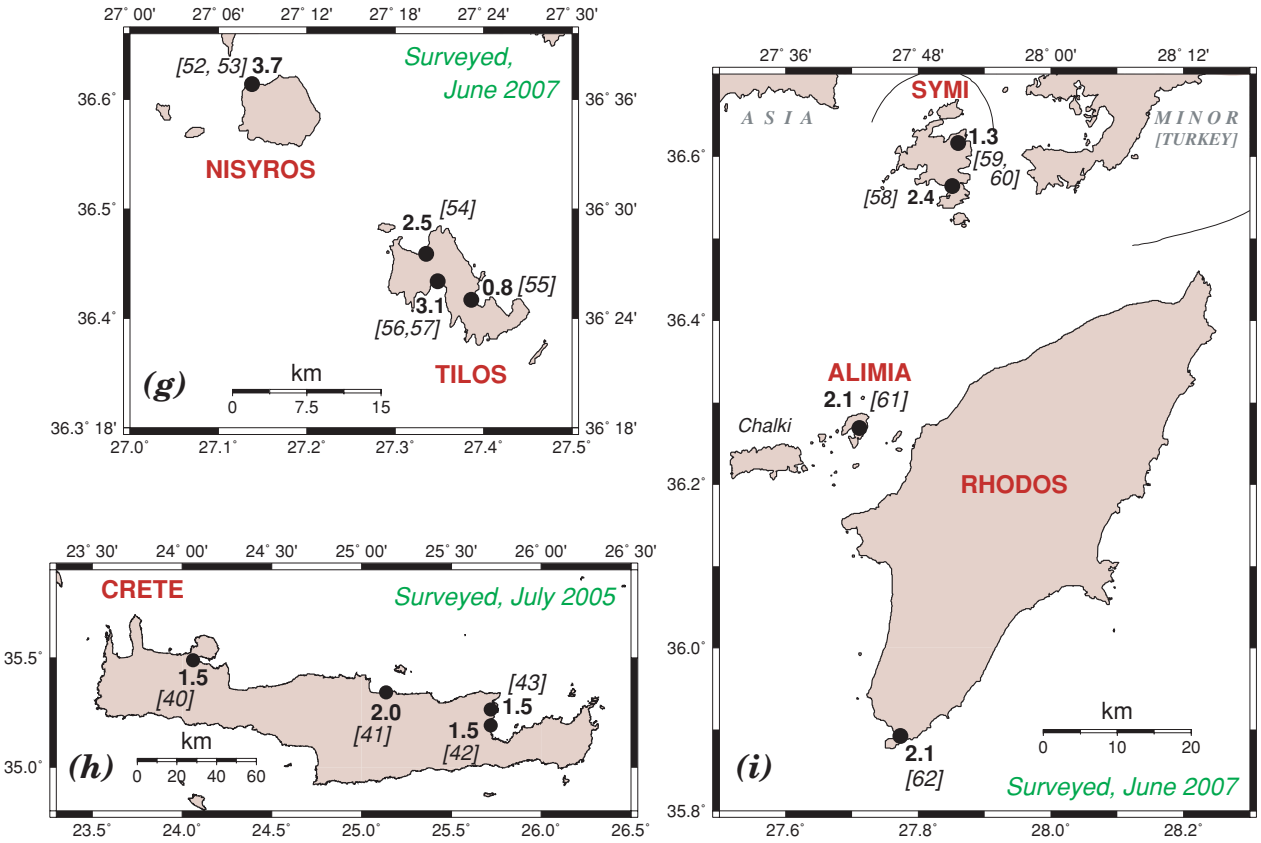

Figure 8. (*Continued*.)

Folegandros, Sites 24–28; Fig. 8(d).

Early reports of run-up reaching 10 m on Folegandros (Galanopoulos 1957) are intriguing since the island is located 80 km west of the epicentre and no similar values were observed on Santorini, at an intermediate distance in a comparable azimuth. We confirmed very high run-up values at two sites on the western coast of the island: At Aggali (Site 25; two witnesses interviewed), it reached 12.6 m, for an inundation distance of 290 m, in what was then a river bed (now occupied by a road), with a substantial flow depth (6.3 m) at the shoreline. Further north, at Ambeli (Site 27), the tsunami was described by a witness as having splashed against a cliff to a height measured at 14.6 m. At the beach of Agios Nikolaos, distant only 850 m from Aggali, the wave penetrated 111 m into an olive grove, running up to a height of 3.1 m. At the other two sites on the island (the port of Karavostasis and the Bay of Agios Georgios), run-up was only 1.3 and 1.1 m, respectively.

Based on the testimony of three eyewitnesses, we thus confirm that waves of exceptional amplitude struck the western shore of Folegandros, in at least two locations. However, those instances were clearly spatially isolated, since run-up was considerably less at Agios Nikolaos and very moderate at the other two sites. There is some suggestion, but no reliable evidence that the waves at Sites 24 and 25 may have been delayed by a few (three?) hours.

Crete; Sites 40–43, Fig. 8(h).

We surveyed five locations on the northern shores of Crete and obtained four eyewitness accounts. In Souda, the port city of Chania in the west of the island, the wave reached up to the radio station, about 350 m inland. This vertical run-up was measured at 1.5 m, while one eyewitness estimated a 0.5 m flow depth. The tsunami had minor impact, as the area was and still is, to this day, sparsely populated due to the proximity to the port and a major naval base.

We could not find any eyewitnesses in Rethymnon, about 60 km east. The local newspaper *Vima* reported on 1956 July 10 that the mean sea level rose about 1 m, and interestingly that it rose further around noon. The paper also reported that sea level in the port oscillated with a period of 10 min and that at times the seafloor of the port became exposed so it was 'walkable'. The 'tide phenomenon' lasted until late in the afternoon.

In Heraklion, 150 km east of Chania, and now the largest city in Crete, the account of one eyewitness was consistent with contemporaneous newspaper reports, that is, the wave flooded the customs house of the port, leading us to measure 2 m run-up and 30 m inundation. During the down-draw, the wave did not overturn any vessels, but came close to doing so. The newspaper *Mesogios* dated 1956 July 10 describes that the oscillations in the port led the passenger ship *Aggelika* to dangerously list against the piers, while vertical motions moved other vessels around causing confusion and fear.

In Agios Nikolaos, 60 km further east, we identified two eyewitnesses and surveyed two sites. Behind the small port, there is an inner lagoon, known as the lake. One eyewitness described how the water level fluctuated up to a level, which we measured at 1.5 m on the north side of the lagoon, at a distance of 5 m from its shoreline. Contemporaneous newspaper reports describe a violent torrent of water passing over the narrow isthmus and into the lagoon, and lake oscillations at a period of 6 min. The modern beach resort of Elunda, northwest of Agios Nikolaos, lies west of a small

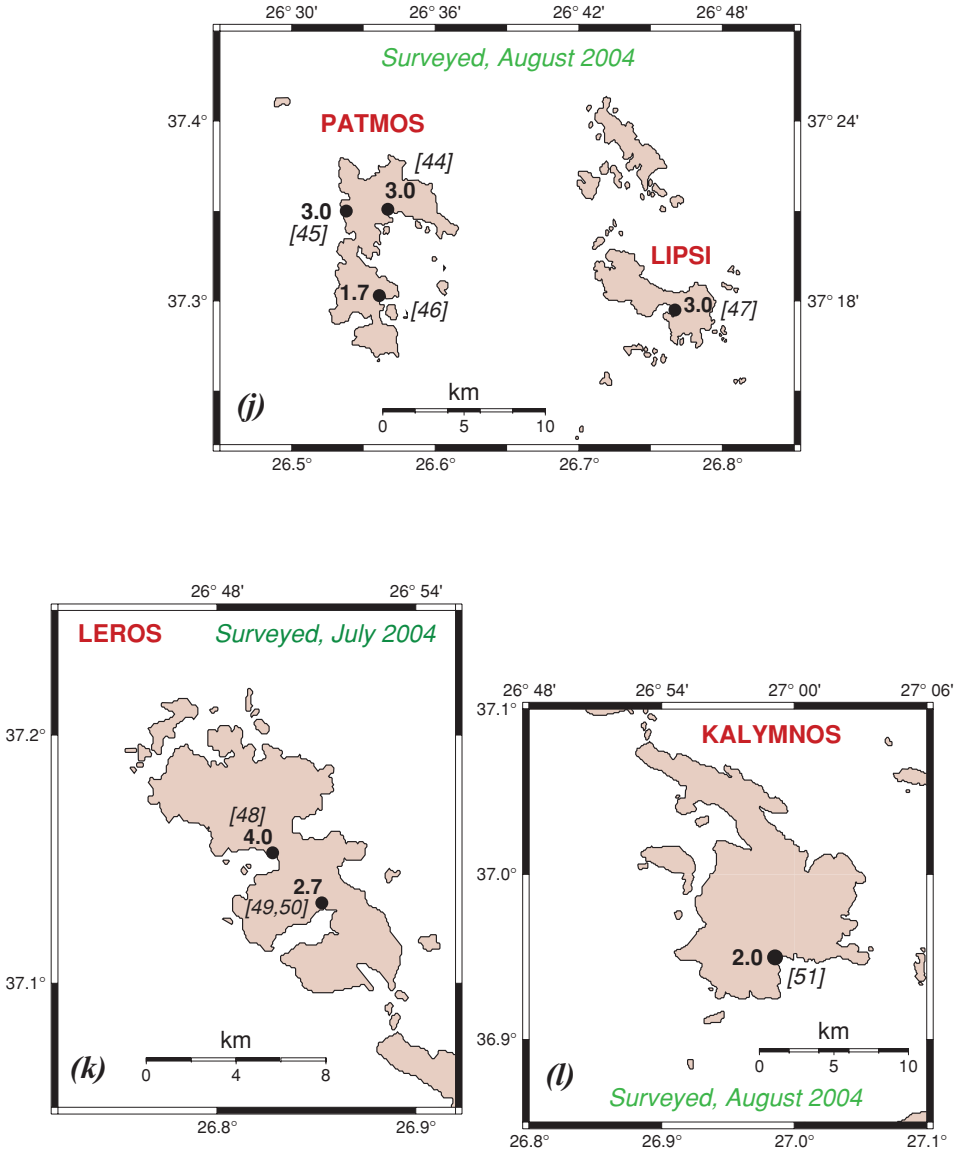

Figure 8. (*Continued*.)

shallow bay fronted by the Spinaloga island, joined to the mainland at the south through a narrow land spit. Based on an eyewitness description, we measured a run up of 1.5 m at Site 43, 150 m inland from where the modern small port now stands. Newspaper accounts reported that the salinas at the west end of the spit were 'destroyed' and quoted a "wave height' there of 2 m.

At the eastern tip of Crete, we investigated two locations. At Sitia, about 40 km east of Agios Nikolaos, local newspapers described a 2-m sea level rise and the movement of steel barrels in the port, caught in surface vortices due to the tsunami currents; however, we have not yet identified witnesses. In Palaikastro, in the course of related work around the local Minoan palace (Bruins *et al.* 2008), an eyewitness pointed to us what we estimated as a penetration of 200 m and run up of 4 m. However, we do not include this datum in our database, for lack of precise GPS surveying.

Patmos; Sites 44–46, Fig. 8(j).

We found three eyewitnesses and measured three data points, the largest flooding extending 200 m inland on the west coast of the island (Site 45). A fourth eyewitness described qualitatively that the flooding washed over the narrow land neck between the town of Patmos and the west, but we consider his report unreliable as we could not confirm it with any of the other three eyewitnesses.

Lipsi; Site 47, Fig. 8(j).

In Lipsi, a small island to the east of Patmos, the wave made a big impression, reaching up to 3 m, as measured along the wall of a tavern at a distance of 10 m from the local quay.

Leros; Sites 48–50, Fig. (8k).

Only a limited amount of time was available to visit the island during an airline connection on the way to Astypalaia. Two points were surveyed in the centre of the main town, Laki, and one on the beach at Gourna, in the western part of the island, where small boats had been deposited by the tsunami on top of olive trees at a distance of 130 m from the shore, indicating a flow depth of 4 m.

Kalymnos; Site 51, Fig. 8(l).

The wave was widely noticed in Kalymnos, with several reports that the seafloor of the port became exposed, with vortices hurtling boats

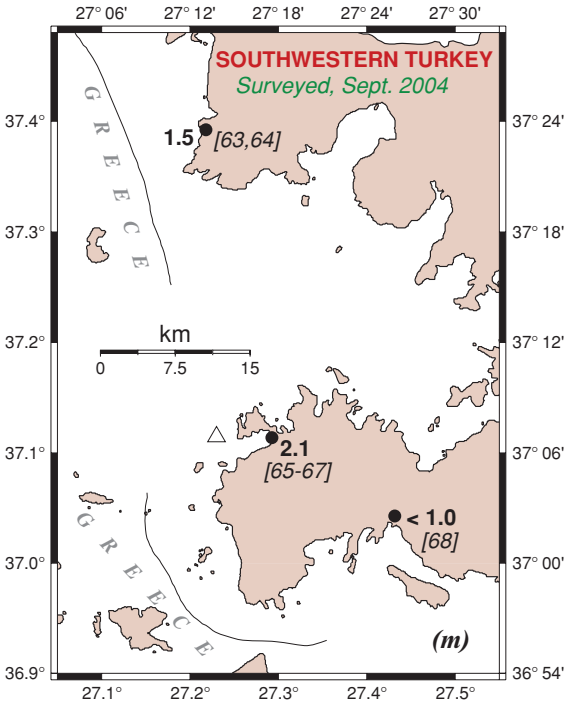

Figure 8. (*Continued*.)

against the quay and against each other. One boat was sunk. Our most credible eyewitness—the only one we found who was able to actually pinpoint a physical location—identified a penetration point, which we measured at 2.2 m and 100 m inland.

Nisyros; Sites 52–53; Fig. 8(g).

On this volcanic island, we located eyewitnesses at the main port in Mandraki and at the fishing village Palloi, both at the north. In Mandraki, one witness reported that the water reached the steps to the post office, that is, a run-up of 2.9 m. Another eyewitness recalled that the wave reached the backyard of her house, 3.7 m above sea level, the phenomenon lasting several hours. In Palloi, locals reported that there was a sandy beach where the small marina is now. They felt a moderate earthquake and recalled the seafloor exposed, but by their own estimates the flooding was not above what they were observing during large storms.

Tilos; Sites 54–57; Fig. 8(g).

The island's port at Livadia, facing NE, has changed significantly since 1956, the old port recently replaced by a small marina. An eyewitness reported that the tsunami reached the level of the old dock, at 0.8 m elevation. In Agios Antonios on the north, the locals recalled that the earthquake was not strongly felt and that reefs were exposed a few minutes later, and the port dried out. Waves reached the beachfront houses, at an elevation of 2.5 m. The eyewitnesses directed us to Eristos, a small fertile valley on the west side that ends upon a long sandy beach. The tsunami overtopped the sand dune at 3.1 m and inundated up to 140 m inland, destroying the crops. We note here that a new road constructed to facilitate access to coastal hotels has resulted in substantial erosion.

Symi; Sites 58–60; Fig. 8(i).

In the harbour of Gialos, eyewitnesses recalled the withdrawal of the waters but no flooding. The waves just reached the entrance of the buildings lying next to the sea. In Pedi, eyewitnesses recalled that the boats in the bay had capsized and indicated that the tsunami reached the entrance of the Agios Georgios church (75 m inland, 1.3 m run-up) and of a present taverna, the phenomenon involving two waves and lasting approximately 30 min. At the famous monastery of Panormitis in the south of the island, one eyewitness remembered that the sea withdrew to the entrance of the bay and then inundated up to the stairs of the monastery (2.4 m run-up).

Alimia; Site 61; Fig. 8(i).

This small island, located NW of Rhodes and east of Chalki, is no longer inhabited. A lone eyewitness from Chalki described how he felt the earthquake and went out of the house, and 'a few minutes later' the water level climbed up to the church of Agios Georgios, at an elevation of 2.1 and 150 m inland. The water level ran down exposing about 100 m of seafloor and the sea remained agitated for several hours.

Rhodos; Site 62; Fig. 8(i).

Due to the size of the island, and the vast recent development along its coast, it was hard to find eyewitnesses among present residents. Only in ancient Kameiros, locals were found who could recall that a tsunami had hit Rhodos, but were unable to point out where the waves had reached. We elected to focus on the peninsula of Prasonissi, at the southern tip of Rhodos, connected to the mainland by a 700-m-long strip of sand, presently less than 100 m at its narrowest point; it is important to note that this sand barrier is a dynamic structure, whose morphology varies significantly through the years, and also features a seasonal change controlled by wave conditions and currents. Local newspapers reported in 1956 that it had been overrun by the tsunami with 9-m flow depths, and 500-m inundation, cutting-off Prasonissi from the mainland. The survey team identified an eyewitness who pointed out the inundation point measured at a smaller run-up of only 2.1 m (Site 62).

Turkish coast; Sites 63–68, Fig. 8(m).

The tsunami was surveyed at three locations along the southwestern coast of Turkey in 2004 September. While the maximum surveyed run-up was moderate (2.1 m at Site 67), the most interesting data were gathered in the town of Yalıkavak, where we were able to interview a group of eleven eyewitnesses at a meeting arranged for us by the town governor in a local coffee house. Of those, at least four remembered the tsunami as having occurred in the 'late morning', probably between 10 and 11 a.m. While this timing cannot be considered as absolute and accurate, the witnesses were systematically and individually cross-examined as to their activities prior to the observation of the tsunami; we were satisfied that two witnesses had a busy workload (e.g. tending to animals, then walking several kilometres back into town) between sunrise and the observation of the tsunami, which makes it highly improbable that the waves arrived at the time expected from our simulations (see next section) for a tsunami generated by, or at the same time as, the earthquake.

5 HYDRODYNAMIC SIMULATIONS

Our modelling was carried out using the MOST numerical code (Titov & Synolakis 1998), which solves the non-linear equations of hydrodynamics under the shallow-water approximation using a finite difference algorithm, and the method of fractional steps (Godunov 1959). Full details can be found in Synolakis (2003). We emphasize that, at the time of writing, MOST is the only code which has been extensively validated through comparisons with laboratory and field data, as per standards and guidelines for numerical codes

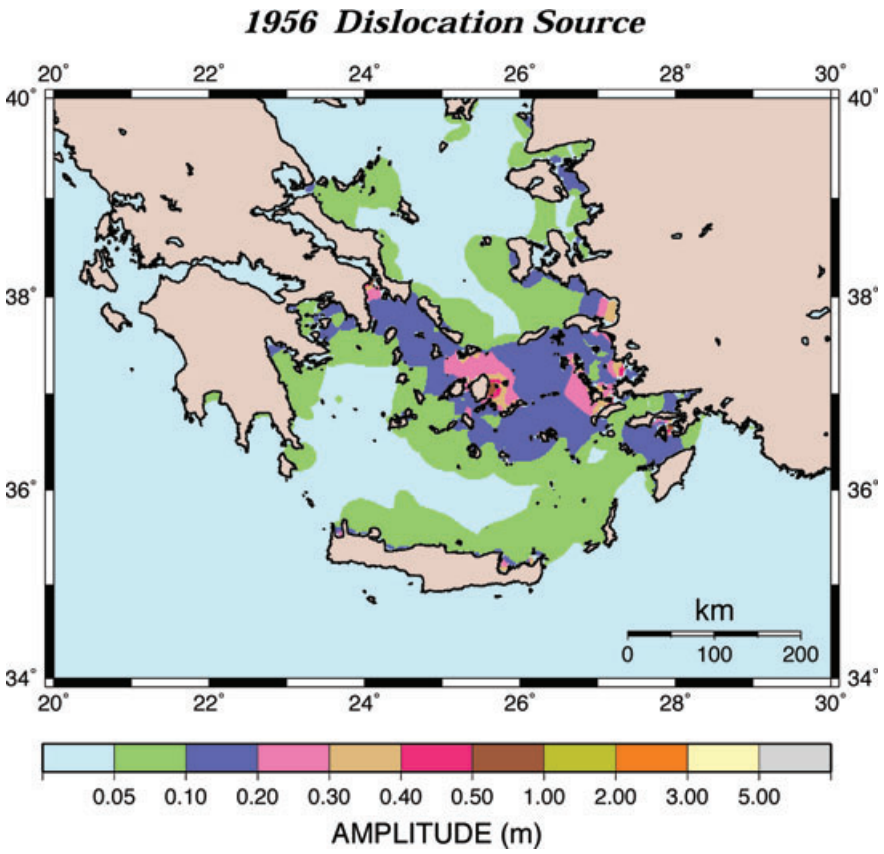

Figure 9. Field of maximum tsunami amplitude, as simulated under the earthquake scenario.

defined by the National Oceanic and Atmospheric Administration for use in computing inundation maps, which have also been adopted by the Nuclear Regulatory Commission of the United States for power-plant sitting studies (Yeh *et al.* 1996; González *et al.* 2007; Synolakis *et al.* 2007; Liu *et al.* 2008).

5.1 Bathymetry

The code is first applied to a coarse grid with a step of 30 arcsec (0.93 km in latitude; 0.74 km in longitude), covering the whole Aegean Sea, from 33°N to 40°N and from 20°E to 31°E. The bathymetry was derived primarily by interpolating the SRTM30 database (Smith & Sandwell 1997), with critical areas around several islands hand-digitized from available marine charts. For inundation calculation at targeted locations (e.g. Amorgos, Folegandros), finer grids were obtained from marine charts of individual harbours and bays, and digitized at a step of 1 arcsec (31 m in latitude; 25 m in longitude).

5.2 Earthquake source

On Fig. 7, we mapped a field of static displacements computed using Mansinha & Smylie's (1971) algorithm, from a source model obtained from our inverted moment tensor, using classical seismic scaling laws (Geller 1976). These values are considered as the initial field of displacement of the sea surface, $\eta(x, y; t = 0_+)$, a legitimate approximation for earthquake sources occurring much faster than the typical period of the tsunami. The field of depth-averaged horizontal velocities is uniformly taken as zero for $t = 0_+$.

The calculation then proceeds with a time step $\delta t = 2.5$ s, satisfying the CFL criterium (Courant *et al.* 1928) for numerical stability on the grid. It is carried out for 5760 time steps or four hours following the earthquake. The solution is saved every 24th step, that is, at intervals of 1 min.

Fig. 9 shows the field of maximum wave amplitude over the area of study, as computed over the coarser grid. These values, usually less than 50 cm, are not meant to be directly compared to the run-up obtained during the field survey and mapped on Fig. 8. A comprehensive simulation of the run-up at all the surveyed sites is simply beyond the scope of this study, since it would require bathymetric and topographic grids on an often-unavailable scale. Rather, we elect to focus our study by examining in detail three sites identified in the field survey as posing an obvious challenge, and for which we were able to obtain fine-scale bathymetry.

1. *Amorgos, Site 6*. A map of the run-up predicted by the earthquake source model around the island of Amorgos is shown on Fig. 10. At Mouros Beach (Site 6), the predicted run-up is only 12 cm, to which one should add the static subsidence of 25 cm. Even so, it remains nearly two orders of magnitude less than surveyed. The reason for this extremely small value is two-fold. First, the largest values of the field of initial displacements are located north of Amorgos (Fig. 7), and the island acts as a barrier for the waves (note that larger run-up is expected on the northern coast). Second, the largest amplitudes simulated at Mouros are negative (i.e. downdraws) which do not contribute to the positive run-up mapped on Fig. 10. At any rate, we note, following Okal & Synolakis (2004), that no amount of adapting the parameters of the earthquake source within physically acceptable bounds can result in a run-up of eight

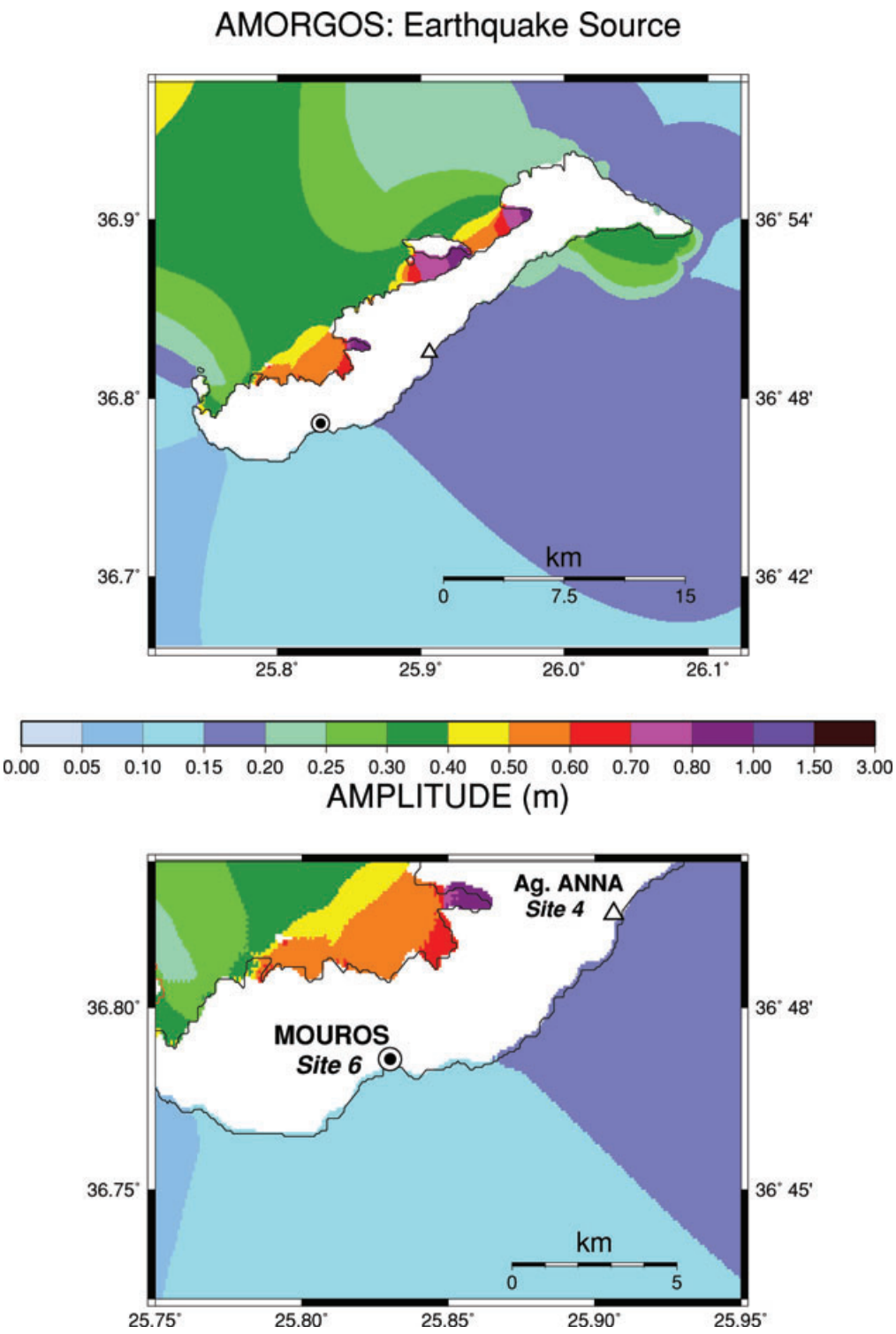

Figure 10. Field of maximum tsunami amplitude (at sea) and run up (on land) for the island of Amorgos, as simulated under the earthquake scenario. The bottom figure is an inset of the vicinity of Sites 4 (Ag. Anna) and 6 (Mouros).

times the fault slip. We conclude that the run-up surveyed at Mouros cannot be explained under the earthquake scenario.

By contrast, on the northern coast of Amorgos, Fig. 8 suggests a run-up value of 80 cm at Agios Pavlos (Site 3). When added to the subsidence predicted by our model (40 cm), this provides an acceptable match to the measured value (1.5 m) at Site 3.

2. *Folegandros, Sites 25 and 26*. A comparable situation occurs at Folegandros, where run-up was surveyed at 12.6 m at Site 25 (Aggali), but only 3.1 m at Agios Nikolaos, only 850 m away. The geometry of the coast is complex, with Site 25 featuring an indentation of the coastline and a small river estuary (in 1956; the stream has now been paved into a road). By contrast, Site 26 is

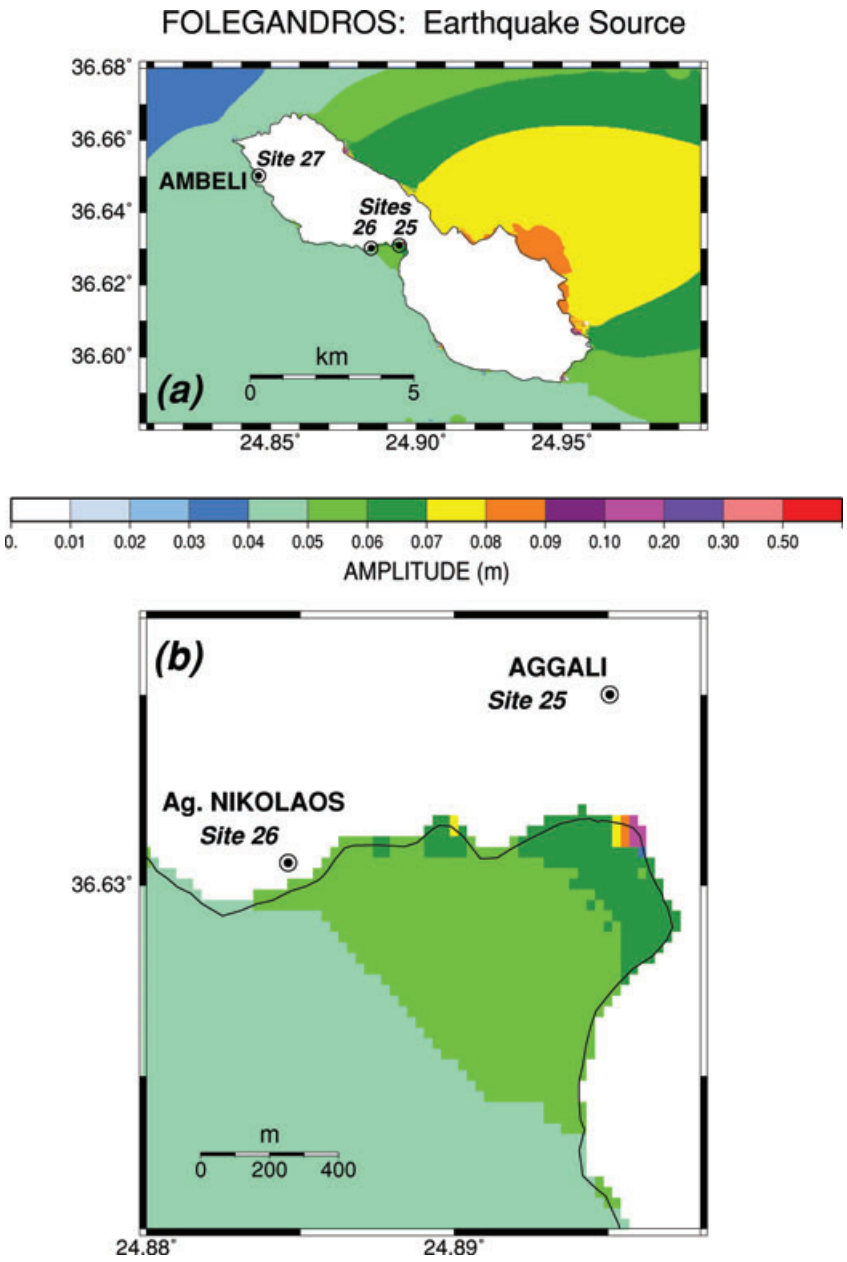

Figure 11. Same as Fig. 10 for the island of Folegandros (a), with close-up of Sites 25 and 26 (b). Note the very small amplitudes predicted under the dislocation scenario. (Figs 10 and 11 use different colour palettes.)

located on a broad, flat alluvial plain occupied by a sparsely planted olive grove. Precise modelling of the run-up under this topography leads to very small values (not exceeding 10 cm at Site 25 and 20 cm on the northeastern coast; Fig. 11), which simply reflects the large distance of the sites from the epicentre (80 km). Once again, it is clear that the earthquake source just cannot explain the magnitude of the run-up surveyed at Site 25.

3. *Yalıkavak (Turkey), Sites 65–67.* Fig. 12 presents a time series of the amplitude of the tsunami simulated under the earthquake scenario at a virtual gauge located just offshore of Yalıkavak, in 30-m deep water (Fig. 8m). It predicts a down-draw starting 33 min after origin time, reaching its maximum 26 min later, and a maximum positive wave expected 99 min after origin time. This corresponds to 05:44, 06:10 and 06:50 local time (GMT +2; only 11 min ahead of solar time), respectively. The initial propagation time of 33 min is in general agreement with fig. 1 of Ambraseys (1960), although that study uses a point source and the exact location of our virtual gauge is masked by a Caption block. Notwithstanding the difficulties inherent in the recollection of time by elderly witnesses interviewed 48 yr after the event, our times are hard to reconcile with the estimates of 10–11 a.m. for the inundation of the coastline, given independently by several witnesses during our interview. Note in particular that the initial wave motion is a down-draw, originating from the negative trough on Fig. 7 and traveling approximately 100 km through the straits between Leros and Lipsi, at an average velocity of $\sim$50 m s^{-1} through the shallow bathymetry of the Eastern Aegean. Delaying the arrival of the wave a minimum of 3 hr would lead to totally unacceptable velocities on the order of only

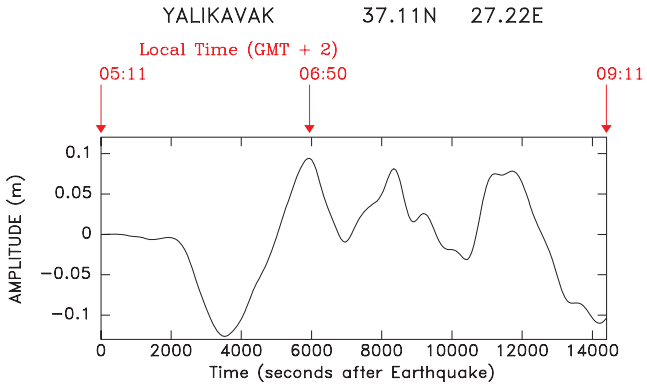

Figure 12. Time series of the numerical simulation of the tsunami generated by the earthquake dislocation for a virtual gauge located at the entrance to the bay of Yalıkavak (triangle on Fig. 8m; depth 30 m).

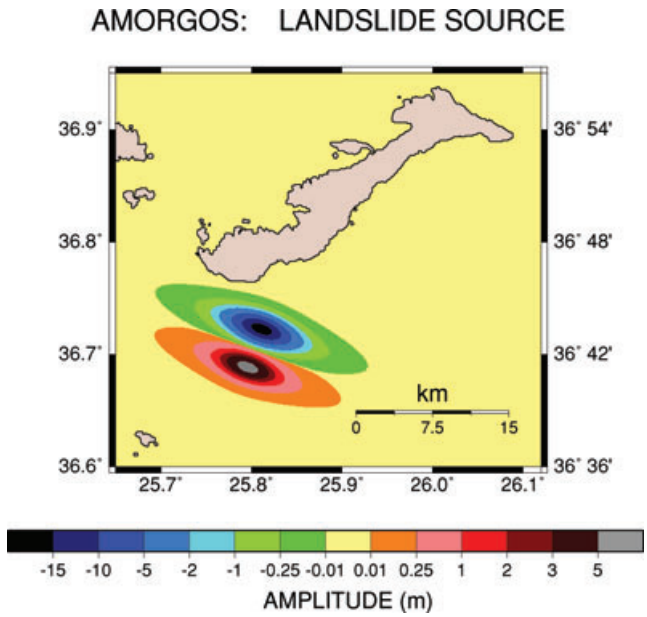

Figure 13. Field of initial state of sea surface used for the simulation under the Amorgos landslide scenario.

8 m s^{-1}. Our simulation confirms that the testimony of our witnesses at Yalıkavak is irreconcilable with the generation of the tsunami by the seismic source.

5.3 Landslide sources

Since the earthquake source fails to account for the run-up values measured at Sites 6 (Mouros, Amorgos) and 25 (Aggali, Folegandros), we simulated a number of landslide scenarios. These were based on simple representations of the initial sea surface field of the form

$$\eta(x, y; t = 0_+) = \{ -\eta_- \cdot \exp(-\alpha_x x^2) + \eta_+ \cdot \exp[-\alpha_x (x - l)^2] \} \cdot \mathrm{sech}^2(\gamma_y \cdot y). \quad (1)$$

This formula describes a dipolar source consisting a of trough of amplitude η_- and a hump of amplitude η_+, separated by a lever of length l in the direction x of the slope of the seafloor, as described by Borrero (2002) and Okal & Synolakis (2004). The width of the poles are controlled by the parameters α_x, and γ_y in the direction y perpendicular to x.

In this study, the parameters of the models were obtained largely by trial and error, and as such, they remain somewhat *ad hoc*. For example, in the case of Folegandros, the slide was localized within the constraints of the local bathymetry to fit the rapid variation of run-up between Sites 25 and 26. The resulting precision is estimated at ∼2 km. The parameters of the slide were inspired from our model of the 1998 Papua New Guinea event (Synolakis *et al.* 2002a), and scaled to fit the observed run-up at Aggali.

In this context, we do not pretend that landslides with those exact geometries did take place, but rather show that we can build landslide models generally comparable to those documented during other tsunamis, which lead to acceptable matches between simulations and observations. Indeed, Perissoratis & Papadopoulos (1999) have documented the presence of underwater slumps in the Amorgos Basin, although their precise dating is unavailable and thus their association with the 1956 event remains circumstantial.

This approach does not directly relate the proposed models to physical constants describing the static (or even dynamic) properties of the proposed landslide (such as volume and density of sediment displaced, maximum velocity of sliding, etc.). Note in this respect that existing empirical laws (Watts 2000; Murty 2003; Bohannon & Gardner 2004) or semi-empirical ones (Synolakis 2003) can produce estimates of the maximum initial wave height varying by more than one order of magnitude, even for the same landslide and even among results derived using the same methodology. On the other hand, our approach has been used successfully in numerical simulations of landslides including the documented events at Ritter Island (1888; Ward & Day 2003), Skagway, Alaska (1994; Synolakis *et al.* 2002b) and Stromboli (2002; Tinti *et al.* 2006), the inferred ones at Unimak, Alaska (1946; Okal *et al.* 2003), Aitape, Papua New Guinea (PNG 1998; Synolakis *et al.* 2002a) and İzmit Bay, Turkey (1999; Yalçıner *et al.* 2000), and the geological-era slides at Etna, Palos Verdes, Goleta and the Farallon Islands (Borrero *et al.* 2001, 2004; Pareschi *et al.* 2006; Uslu 2008). Recently, Billi *et al.* (2008) have used backtracking of tsunami rays from a data set of arrival times compiled in the aftermath of the 1908 Messina tsunami, to propose that its source was a landslide in the Ionian Sea; although different in scope, their approach shares with ours its generally *ad hoc* character, namely that a landslide is required because no acceptable earthquake source can explain the characteristics of the tsunami.

It is in this general framework that we use landslide models to simulate our observations at Amorgos and Folegandros. Because large run-up amplitudes are concentrated in the immediate vicinity of landslide sources, distinct sources are necessary to explain the large run-up heights observed on the two islands, at locations separated by 85 km.

1. *Amorgos.* Fig. 13 shows the initial sea-surface deformation under the Amorgos landslide scenario; the source is located ∼10 km from the southwestern tip of Amorgos. It features a negative trough ($\eta_- = 18$ m) and a positive hump ($\eta_+ = 6$ m), separated by a lever $l = 4$ km, in the direction $x =$ N200°E, with tapering parameters $\alpha_x = 0.8$ km^{-2} and $\gamma_y = 0.4$ km^{-1}. This slump, on the order of 5 km^3 in volume, could be comparable to that involved during the 1998 PNG disaster (Synolakis *et al.* 2002a). As shown on Fig. 14, the resulting simulation reproduces several key features of our survey. First, extreme run-up (in excess of 7 m) is concentrated on the southernmost part of the island; the northern coast is unaffected. Second the run-up is maximum in the vicinity of Site 6 (Mouros)

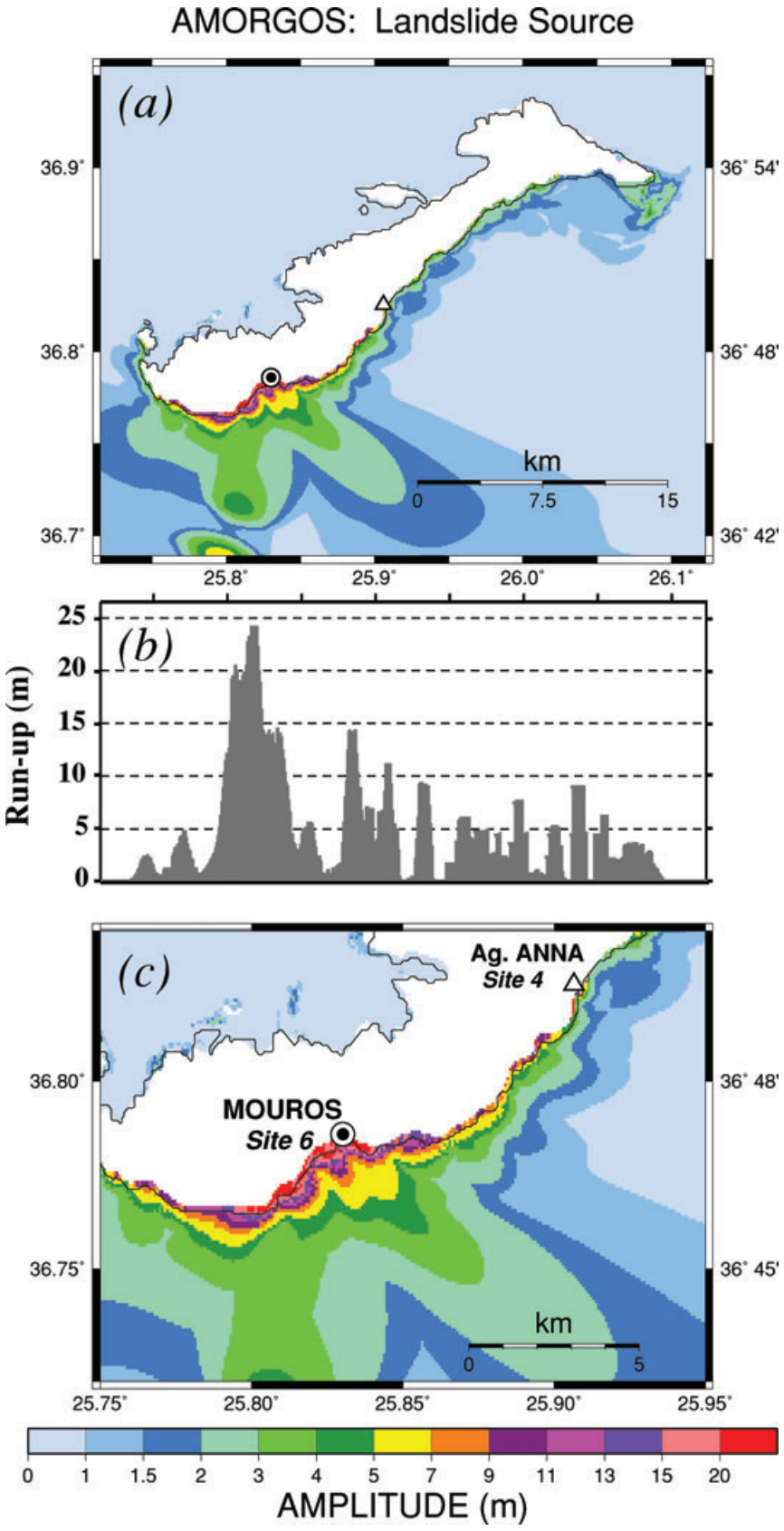

Figure 14. (a) Same as Fig. 10a, under the Amorgos landslide scenario. (b) Simulated runup along the southern coast of Amorgos, plotted as a function of longitude using the same scale as in (a). (c) Close-up of (a) in the vicinity of Sites 4 and 6.

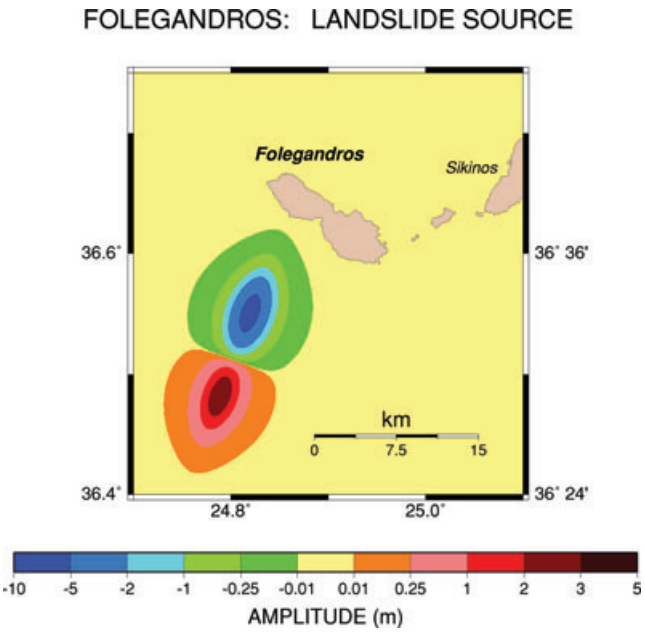

Figure 15. Field of initial state of sea surface used for the simulation under the Folegandros landslide scenario.

where it reaches a maximum value of 24 m, in general agreement with our surveyed value. Finally, the run-up at Site 4 (Agia Anna) remains under 10 m, which is also in agreement with the wave having not reached the chapel. By contrast, Fig. 14 shows that the landslide source has an essentially negligible contribution on the northern coast of Amorgos, and in particular at Agios Pavlos (Site 3; 6 cm), where the run-up was explained satisfactorily by the dislocation source.

This model differs significantly from Perissoratis & Papadopoulos' (1999), who suggested that the 1956 tsunami was generated by massive NW-trending slumping of the coast of Anafi (note an obvious typographic error in their estimate of only a few million metre cubes for its volume). Under their scenario, catastrophic amplitudes would have been recorded on Anafi, rather than Amorgos, the tsunami would not have appeared as a leading depression on Amorgos, and the run-up would not fall off drastically between Sites 6 and 4.

2. *Folegandros*. We examined many possible models of submarine landslides off the southwestern coast of Folegandros, and selected the scenario shown on Fig. 15, which involves a generally smaller slide ($\eta_- = 7$ m; $\eta_+ = 3$ m; $\alpha_x = 0.1$ km^{-2}; $\gamma_y = 0.7$ km^{-1}) displaced along a longer lever $l = 8$ km, in the azimuth N200°E, generally compatible with the local slope of the bathymetry. The results of our simulations, presented on Fig. 16, give acceptable matches to the run-up values documented at Site 25 (12.6 m) and 26 (3.1 m). In addition, the landslide leaves the northern shore of the island unaffected. At Site 27 (Ambeli), the predicted run-up of 9 m falls short of the observed value (14.6 m); however, the site involved a splash on a very steep cliff, which is not modelled properly under the MOST code. Finally, our model would also predict consistently large amplitudes (in the 5–11 m range) along the southeastern shore the island, but this corresponds to a rugged portion of coastline, bearing no settlements and in which we were unable to obtain data points based on witness testimonies.

In conclusion of this section, we have established that the field of static sea floor displacements generated by the source of the Amorgos earthquake is insufficient to explain the run-up observed at several key locations, notably Mouros on the southern coast of Amorgos and Aggali on the western shore of Folegandros. On the other hand, the observations of our witnesses can be reconciled with inundation simulations using reasonable, if somewhat *ad hoc*, models of submarine landslides, which we interpret as having been triggered by the earthquake. It is probable that a similar scenario is responsible for the relatively large amplitudes surveyed on the northern shore of Astypalaia (Site 19).

In the case of Sites 65–67 (Yalıkavak, Turkey), the time discrepancy illustrated on Fig. 12 similarly suggests as the source of the local waves an ancillary phenomenon, most probably a submarine landslide, since no large enough aftershock occurred in an adequate time frame. However, given the smaller amplitudes involved, we could not obtain useful constraints on its possible source parameters. Under this model, the trigger of the landslide by the earthquake would be delayed approximately three hours (or less if triggered by an aftershock). A delay of ∼1.5 hr was proposed under a similar scenario in the case of the large 1945 Makran earthquake and tsunami (Ambraseys & Melville 1982), and a much shorter one (duration: 13 min) was documented in the case of the 1998 PNG tsunami (Synolakis *et al.* 2002a); due the complex, non-linear, and generally poorly understood, nature of the triggering process of a landslide, such delays are expected to vary, and could reach a few hours, a value certainly typical of the interval separating, for example, a main shock from a strong aftershock.

6 CONCLUSIONS

With the use of modern seismological techniques, we have conducted a comprehensive investigation of the source of the 1956 Amorgos earthquake, the largest one to have stricken Greece in the past 100 yr. In particular, we settle the still unresolved question of its focal mechanism, which is found to express extensional stress across the backarc basin in the Aegean Sea. Aftershock relocations define a fault zone extending 75 km × 40 km, and suggest that the fault plane is the one shallow-dipping to the southeast. The seismic moment, $M_0 = 3.9 \times 10^{27}$ dyn cm, is greater than that of any event having occurred in the Mediterranean since the dawn of the digital era (1976).

Using the methods developed during our previous work on the 1946 Aleutian tsunami, we have compiled a homogeneous data set of 68 surveyed run-up values on 16 islands and in Asia Minor, based on the interview of elderly witnesses of the tsunami. We confirm the occasional occurrence of very large run-up amplitudes (20 m on Amorgos; 13 m on Folegandros; 10 m on Astypalaia), but also their exceptional character, most of the run-up otherwise not exceeding 4 m.

Our numerical simulations confirm the longstanding suggestion, first expressed by Galanopoulos (1957) and Ambraseys (1960), that the occurrence of high-amplitude run-up along localized segments of shoreline (Amorgos, Folegandros, and probably Astypalaia) reflect the triggering of underwater landslides by the main shock or possibly its aftershocks, as suggested by inconsistencies in time reported to us by witnesses (e.g. on the Turkish coast). Although the models used in Section 5 do not claim to be definitive representations of the actual landslides having generated the highest run-ups, they demonstrate that the main characteristics of the latter (amplitude and spatial extent) can be successfully reproduced using underwater landslides featuring acceptable parameters, extrapolated

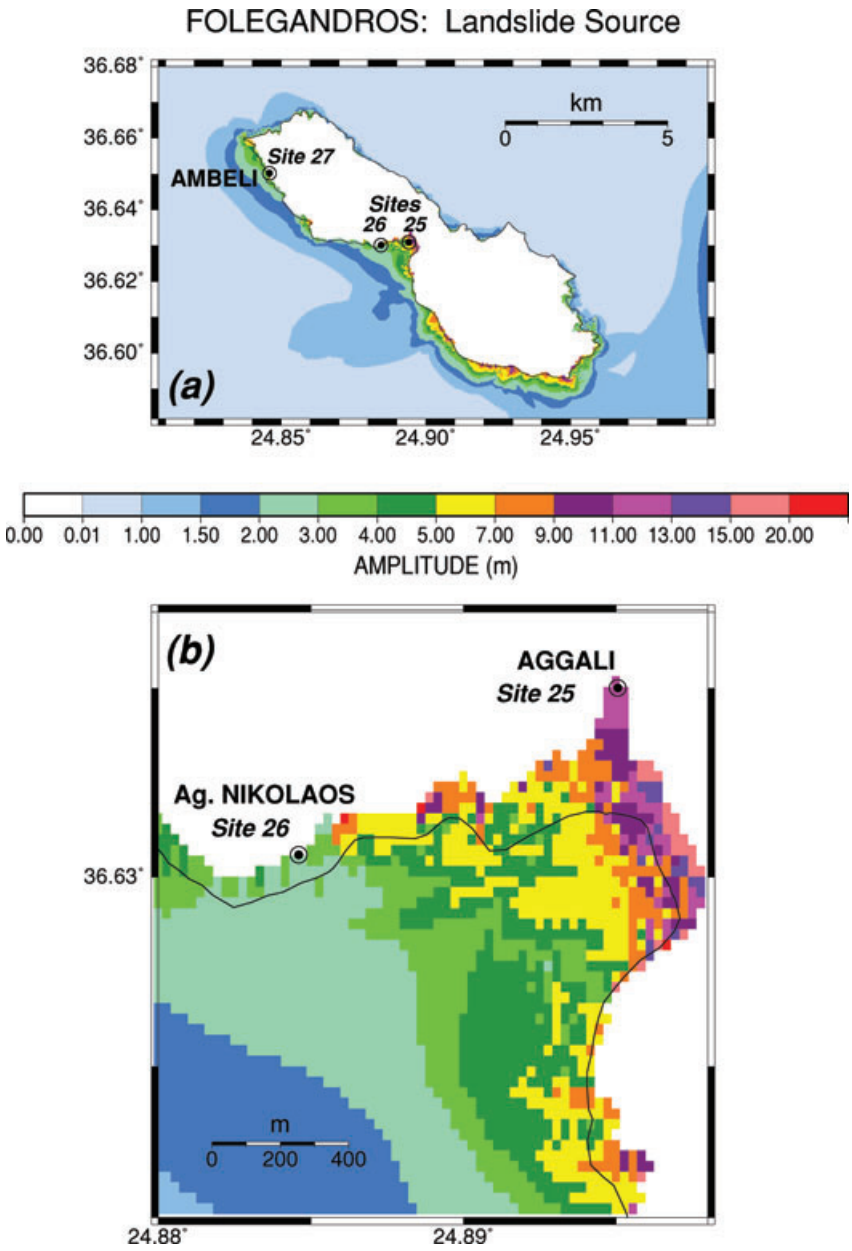

Figure 16. Same as Fig. 11, under the Folegandros landslide scenario.

from models of case studies having provided better documented data sets, such as the PNG disaster (Synolakis *et al.* 2002a).

In conclusion, our study reaffirms the primary importance, in the Aegean Basin, of landslides in terms of tsunami hazard following a large earthquake, as suggested independently in the different tectonic context of the Gulf of Corinth by Stefatos *et al.* (2006). While in 1956 the remote character of the relevant sections of coastline prevented the waves from inflicting heavy damage or casualties, recent development, such as on the beach front at Aggali (Folegandros) or at the modern marinas at Elunda (Crete) or Bodrum (Turkey), would considerably increase hazard under a similar scenario. Finally, the probable temporal discrepancy between the earthquake source and the arrival of the tsunami on the Turkish Coast (Sites 65–67) underlines the non-linear character of the triggering process, and the resulting unpredictability of its timing, which only adds to the ultimate hazard borne by a tsunami generated by a landslide in the aftermath of a seismic event.

ACKNOWLEDGMENTS

This study was supported by the National Science Foundation under Grants CMS-03-01054 to EAO and CMS-03-01081 to CES, and by a 'TRANSFER' grant of the European Union to the Institute of Applied and Computational Mathematics of the Foundation of Research and Technology of Hellas (FORTH). Fieldwork was partially supported by the Howland Fund of the Department of Earth & Planetary Sciences, Northwestern University. We are grateful to John Ebel, Don Helmberger and James Dewey for providing copies

of, or access to, historical seismograms. We acknowledge help in the field from Ahmet C. Yalçıner at the Turkish sites, Maria Gaspari in Folegandros and Crete and Spiros Fotinis in Naxos. The paper was improved by the thoughtful comments of two anonymous reviewers. Most maps were drafted using the GMT software (Wessel & Smith 1991).

REFERENCES

Ambraseys, N.N., 1960. The seismic sea wave of July 9, 1956 in the Greek archipelago, *J. geophys. Res.,* **65,** 1257–1265.

Ambraseys, N.N. & Jackson, J.A., 1990. Seismicity and associated strain of central Greece between 1890 and 1988, *Geophys. J. Int.,* **101,** 663–708.

Ambraseys, N.N. & Jackson, J.A., 1998. Faulting associated with historical and recent earthquakes in the Eastern Mediterranean region, *Geophys. J. Int.,* **133,** 390–406.

Ambraseys, N.N. & Melville, C.P., 1982. *A History of Persian Earthquakes,* Cambridge Univ. Press, Cambridge, 219 pp.

Billi, A., Funicello, R., Minelli, L., Faccenna, C., Neri, G., Orecchio, B. & Presti, D., 2008. On the cause of the 1908 Messina tsunami, Southern Italy, *Geophys. Res. Lett.,* **35**(6), L06301, doi:10.1029/2008GL033251.

Bohannon, R.G. & Gardner, J.V., 2004. Submarine landslides of San Pedro Escarpment, southwest of Long Beach, California, *Mar. Geol.,* **203,** 1261–1268.

Borrero, J.C., 2002. Tsunami hazards in Southern California, *Ph.D. thesis*. University of Southern, California, Los Angeles, 306 pp.

Borrero, J.C., Dolan, J. & Synolakis, C.E., 2001. Tsunami sources within the Eastern Santa Barbara Channel, *Geophys. Res. Lett.,* **28,** 643–647.

Borrero J.C., Legg, M.R. & Synolakis, C.E., 2004. Tsunami sources in the Southern California Bight, *Geophys. Res. Lett.,* **31**(13), L13211, doi:10.1029/2004GL020078.

Bruins, H.J., MacGillivray, J.A., Synolakis, C.E., Benjamini, C., Keller, J., Kisch, H.J., Klügel, A. & Van Der Plicht, J., 2008. Geoarcheological tsunami deposits at Palaikastro (Crete), and the Late Minoan IA eruption of Santorini, *J. Archeol. Sci.,* **35,** 191–212.

Courant, R., Friedrichs, K. & Lewy, H., 1928. Über die partiellen Differenzengleichungen der mathematischen Physik, *Mathematische Annalen,* **100,** 32–74.

Dominey-Howes, D., Cundy, A. & Croudace, I., 2000. High-energy marine flood deposits on Astypalaea Island, Greece: possible evidence for the AD 1956 southern Aegean tsunami, *Mar. Geol.,* **163,** 303–315.

Engdahl, E.R. & Villaseñor, A., 2002. Global seismicity: 1900–1999, in *International Handbook of Earthquake and Engineering Seismology, Part A,* Chapter 41, pp. 665–690, eds Lee, W.H.K., Kanamori, H., Jennings, P.C., Kisslinger, C., Academic Press, Boston.

Galanopoulos, A.G., 1957. The seismic sea wave of 9 July 1956, *Prakt. Akad. Athens,* **32,** 90–101 (in Greek).

Geller, R.J., 1976. Scaling relations for earthquake source parameters and magnitudes, *Bull. seism. Soc. Am.,* **66,** 1501–1523.

Godunov, S.K., 1959. Finite difference methods for numerical computations of discontinuous solutions of the equations of fluid dynamics, *Matemat. Sbornik,* **47,** 271–295.

González, F.I. *et al*., 2007. Scientific and technical issues in tsunami hazard assessment of nuclear power plant sites. *NOAA Tech. Memo. OAR PMEL-136, NTIS: PB2008-101460,* NOAA Pac. Mar. Envir. Lab., 125 pp., Seattle.

Kagan, Y.Y., 1991. 3-D rotation of double-couple earthquake sources, *Geophys. J. Int.,* **106,** 709–716.

Le Pichon, X. & Angelier, J., 1979. The Hellenic arc and trench system: a key to the neotectonic evolution of the Eastern Mediterranean area, *Tectonophysics,* **60,** 1–42.

Liu, P.L.-F., Yeh, H. & Synolakis, C.E. (Eds.), 2008. Advanced numerical models for simulating tsunami waves and runup, in *Adv. Coastal Ocean Ang.,* Vol. **10**, World Scientific Publishing, Singapore.

López, A.M. & Okal, E.A., 2006. A seismological reassessment of the source of the 1946 Aleutian 'tsunami' earthquake, *Geophys. J. Int.,* **165,** 835–849.

Mansinha, L. & Smylie, D.E., 1971. The displacement fields of inclined faults, *Bull. seism. Soc. Am.,* **61,** 1433–1440.

McKenzie, D., 1972. Active tectonics of the Mediterranean region, *Geophys. J. Roy. astr. Soc.,* **30,** 109–185.

Murty, T.S., 2003. Tsunami wave height dependence on landslide volume, *Pure appl. Geophys.,* **160,** 2147–2153.

Okada, Y., 1985. Surface deformation due to shear and tensile faults in a half-space. *Bull. seism. Soc. Am.,* **75,** 1135–1154.

Okal, E.A. & Hébert, H., 2007. Far-field modeling of the 1946 Aleutian tsunami, *Geophys. J. Int.,* **169,** 1229–1238.

Okal, E.A. & Reymond, D., 2003. The mechanism of the great Banda Sea earthquake of 01 February 1938: applying the method of Preliminary Determination of Focal Mechanism to a historical event, *Earth planet. Sci. Lett.,* **216,** 1–15.

Okal, E.A. & Synolakis, C.E., 2004. Source discriminants for near-field tsunamis, *Geophys. J. Int.,* **158,** 899–912.

Okal, E.A. *et al*., 2002. A field survey of the 1946 Aleutian tsunami in the far field, *Seismol. Res. Lett.,* **73,** 490–503.

Okal, E.A., Plafker, G., Synolakis, C.E. & Borrero, J.C., 2003. Near-field survey of the 1946 Aleutian tsunami on Unimak and Sanak Islands, *Bull. seism. Soc. Am.,* **93,** 1226–1234.

Papadopoulos, G.A. & Pavlides, S.B., 1992. The large 1956 earthquake in the South Aegean: macroseismic field configuration, faulting, and neotectonics of Amorgos Island, *Earth planet. Sci. Lett.,* **113,** 383–396.

Papastamatiou, J., Zachos, K. & Voutetakis, S., 1956. The earthquake of Santorini of 9 July 1956, *Rept. Athens Inst. Geol. Subsurface*.

Papazachos, B.C. & Delibassis, N.D., 1969. Tectonic stress field and seismic faulting in the area of Greece, *Tectonophysics,* **7,** 231–255.

Papazachos, B.C., Koutitas, Ch., Hadzidimitriou, P.M., Karacostas, B.G. & Papaioannou, Ch.A., 1985. Source and short-distance propagation of the July 9, 1956 Southern Aegean tsunami, *Mar. Geol.,* **65,** 343–351.

Pareschi, M.T., Boschi, E., Mazzarini, F. & Favalli, M., 2006. Large submarine landslides offshore Mount Etna, *Geophys. Res. Lett.,* **33**(13), L13302, doi:10.1029/2006GL026064.

Pedersen, G., Gjevik, B., Harbitz, C.B., Dybesland, E., Johnsgard, H. & Langtangen, H.P., 1995. GITEC Final Scientific Report (Chapter Nine), in *The Genesis and Impact of Tsunamis on the European Coasts, Final Scientific Report,* ed. Tinti, S., General Directorate XII, European Union.

Perissoratis, C. & Papadopoulos, G., 1999. Sediment instability and slumping in the Southern Aegean Sea and the case history of the 1956 tsunami, *Mar. Geol.,* **161,** 287–305.

Reymond, D. & Okal, E.A., 2000. Preliminary determination of focal mechanisms from the inversion of spectral amplitudes of mantle waves, *Phys. Earth planet. Inter.,* **121,** 249–271.

Ritsema, A.R., 1974. Earthquake mechanisms of the Balkan region, *Kon. Ned. Meteor. Inst. Repts.,* **74**(4), 36 pp.

Romanowicz, B.A. & Suárez, G., 1983. An improved method to obtain the moment tensor depth of earthquakes from the amplitude spectrum of Rayleigh waves, *Bull. seism. Soc. Am.,* **73,** 1513–1526.

Shirokova, E.I., 1972. Napryazheniya i razryvy v ochagakh zemletryasenii Sredizemnomorskovo-Aziatskovo seismicheskovo poyasa, in *Polye uprugikh napryazhenii zemli i mekhanizm ochagov zemletryasenii,* pp. 112–148, eds Balakina, L.M., Vvedenskaya, A.V., Golubeva, N.V., Misharina, L.A., Shirokova, E.I., Akad. Nauk SSSR, Moskva (in Russian).

Smith, W.H.F. & Sandwell, D.T., 1997. Global sea floor topography from satellite altimetry and ship depth soundings, *Science,* **277,** 1956–1962.

Solov'ev, S.L., Solov'eva, O.N., Go, Ch.N., Kim, Kh.S. & Shchetnikov, N.A., 2000. *Tsunamis in the Mediterranean Sea, 2000 B.C. – 2000 A.D.,* Kluwer, Dordrecht, 237 pp.

Stefatos, A., Charalambakis, M., Papatheodorou, G. & Ferentinos, G., 2006. Tsunamigenic sources in an active European half-graben (Gulf of Corinth, Central Greece), *Mar. Geol.,* **232,** 35–47.

Stein, R.S., Barka, A.A. & Dieterich, J.H., 1997. Progressive failure on the North Anatolian fault since 1939 by earthquake stress triggering, *Geophys. J. Int.,* **128,** 594–604.

Stiros, S.C., Marangou, L. & Arnold, M., 1994. Quaternary uplift and tilting of Amorgos Island (Southern Aegean) and the 1956 earthquake, *Earth planet. Sci. Lett.,* **128,** 65–76.

Synolakis, C.E., 2003. Tsunami and seiche, in *Earthquake Engineering Handbook,* eds Chen, W.-F., Scawthron, C., pp. 9_1–9_90, CRC Press, Boca Raton.

Synolakis, C.E. & Okal, E.A., 2005. 1992–2002: perspective on a decade of post-tsunami surveys, in *Tsunamis: Case Studies and Recent Developments,* Vol. **23:** Adv. Natur. Technol. Hazards, pp. 1–30, ed. Satake, K., Springer, Dordrecht.

Synolakis, C.E., Bardet, J.-P., Borrero, J.C., Davies, H.L., Okal, E.A., Silver, E.A., Sweet, S. & Tappin, D.R., 2002a. The slump origin of the 1998 Papua New Guinea tsunami, *Proc. Roy. Soc. (London), Ser. A,* **458,** 763–789.

Synolakis, C.E., Yalçıner, A.C., Borrero, J.C. & Plafker, G., 2002b. Modeling of the November 3, 1994 Skagway, Alaska tsunami, in *Solutions to Coastal Disasters '02,* pp. 915–927, eds Ewing, L., Wallendorf, L., Amer. Soc. Civil Eng., Reston, VA.

Synolakis, C.E., Bernard, E.N., Titov, V.V., Kánoğlu, U. & González, F.I., 2007. Standards, criteria, and procedures for NOAA evaluation of tsunami numerical models, *NOAA Tech. Memo. OAR PMEL-135, NTIS: PB2007–109601*, NOAA Pac. Mar. Envir. Lab., Seattle, 55 pp.

Taymaz, T., Jackson, J. & McKenzie, D., 1991. Active tectonics of the north and central Aegean Sea, *Geophys. J. Intl.,* **106,** 433–490.

Tinti, S., Pagnoni, G. & Zaniboni, F., 2006. The landslides and tsunamis of the 30th of December 2002 in Stromboli analysed through numerical simulations, *Bull. Volcanol.,* **68,** 462–479.

Titov, V.V. & Synolakis, C.E., 1998. Numerical modeling of tidal wave runup, *J. Waterw. Port, Coastal Ocean Eng.,* **124,** 157–171.

Uslu, B., 2008. Deterministic and probabilistic tsunami studies in California from near- and far-field sources, *Ph.D. thesis*. Univ. Southern Calif., Los Angeles.

Ward, S.N. & Day, S., 2003. Ritter Island Volcano lateral collapse and the tsunami of 1888, *Geophys. J. Int.,* **154,** 891–902.

Watts, P., 2000. Tsunami features of solid block underwater landslides, *J. Watwy. Port Coast. Oc. Eng.,* **126,** 144–152.

Wessel, P. & Smith, W.H.F., 1991. Free software helps map and display data, *Eos, Trans. Amer. Geophys. Un.,* **72,** 441 and 445–446.

Wysession, M.E., Okal, E.A. & Miller, K.L., 1991. Intraplate seismicity of the Pacific Basin, 1913–1988, *Pure appl. Geophys.,* **135,** 261–359.

Yalçıner, A.C., Altınok, Y. & Synolakis, C.E., 2000. Tsunami waves in İzmit Bay after the Kocaeli earthquake, *Earthq. Spectra,* **16**(Suppl. A.), 55–62.

Yeh, H., Liu, P.L.-F. & Synolakis, C.E. (eds), 1996. *Long-wave Runup Models,* World Scientific Publishing, Singapore, 403 pp.